JOC The Journal of Organic Chemistry

Article

pubs.acs.org/joc

Density Functional Theory Calculations in Stereochemical Determination of Terpecurcumins J–W, Cytotoxic Terpene-Conjugated Curcuminoids from *Curcuma longa* L.

Xionghao Lin,[†] Shuai Ji,[†] Xue Qiao,[†] Hongbo Hu,[‡] Ni Chen,[‡] Yinhui Dong,[‡] Yun Huang,[†] Dean Guo,[†] Pengfei Tu,[†] and Min Ye*[,†]

[†]State Key Laboratory of Natural and Biomimetic Drugs, School of Pharmaceutical Sciences, Peking University, 38 Xueyuan Road, Beijing 100191, China

[‡]College of Food Science and Nutritional Engineering, China Agricultural University, 17 Qinghua East Road, Beijing 100083, China

Supporting Information

ABSTRACT: Fourteen novel terpene-conjugated curcuminoids, terpecurcumins J–W (**1**–**14**), have been isolated from the rhizomes of *Curcuma longa* L. Among them, terpecurcumins J–Q and V represent four unprecedented skeletons featuring an unusual core of hydrobenzannulated[6,6]-spiroketal (**1** and **2**), bicyclo[2.2.2]octene (**3**–**7**), bicyclo[3.1.3]octene (**8**), and spiroepoxide (**13**), respectively. The structures of compounds **1**–**14** were elucidated by extensive spectroscopic analysis, and their absolute configurations were established by electronic circular dichroism, vibrational circular dichroism, and ^{13}C NMR spectroscopic data analysis, together with density functional theory calculations. The structure and configuration of **1** was further confirmed by single-crystal X-ray diffraction (Cu Kα). The biogenetic pathways of **1**–**14** were proposed, involving Michael addition, condensation, Diels–Alder cycloaddition, and electrophilic substitution reactions. Terpecurcumins showed more potent cytotoxic activities than curcumin and ar-/β-turmerone. Among them, terpecurcumin Q (**8**) exhibited IC_{50} of 3.9 μM against MCF-7 human breast cancer cells, and mitochondria-mediated apoptosis played an important role in the overall growth inhibition. Finally, LC/MS/MS quantitative analysis of five representative terpecurcumins indicated these novel compounds were present in *C. longa* at parts per million level.

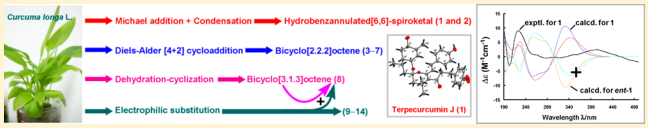

INTRODUCTION

The global burden of cancer has been growing each year.[1] On the other hand, effective drugs for the prevention and treatment of cancer are still in shortage.[2,3] Therefore, the exploration of new oncology drugs with fewer adverse reactions remains a big challenge for pharmaceutical chemists. Given their unique structures, natural products are a major source for the discovery of oncology drugs.[4]

Turmeric is derived from the rhizomes of *Curcuma longa* L. (Zingiberaceae family). It is a popular natural spice and a well-known Chinese herbal medicine. The major chemical constituents of turmeric are curcuminoids and terpenes, which exhibit diverse biological activities, including anticancer, anti-inflammatory, antioxidant, and antiviral activities.[5,6] Among them, the most abundant and intensively studied is curcumin, one of the most well-known natural products as a promising anticarcinogenic agent.[7−9] Recently, we isolated a series of minor compounds terpecurcumins A–I from *C. longa*, which represented a series of structures conjugating curcuminoids with sesquiterpenes through C–C or C–O–C bond.[10] Similar structures were also reported by Huang and co-workers.[11,12] Interestingly, some of these new compounds showed higher cytotoxic activities than curcumin against human cancer cells.

In our continued efforts to discover anticancer compounds from *C. longa*, terpecurcumins J–W (**1**–**14**) (Figure 1) were isolated from a less polar fraction of turmeric extract. Among them, compounds **1**–**8** and **13** possess four unprecedented skeletons that are structurally distinct from the previously reported terpecurcumins A–I.[10] The structures of **1**–**14** were identified on the basis of extensive spectroscopic analysis, and their absolute configurations were unambiguously established by single-crystal X-ray diffraction (for **1**) and quantum chemical calculations including electronic circular dichroism (ECD), vibrational circular dichroism (VCD), and ^{13}C NMR spectra prediction. Terpecurcumins represent a new class of turmeric compounds and indicate novel biosynthetic pathways. In this paper, we report the isolation, structural elucidation, plausible biogenetic pathways, quantitative analysis, and cytotoxic activities of terpecurcumins J–W.

RESULTS AND DISCUSSION

Structural Elucidation and Absolute Configuration of Terpecurcumins J–W (1–14). Terpecurcumin J (**1**) has a molecular formula of $C_{34}H_{40}O_6$ as established by positive HRESIMS ($[M + H]^+$ m/z 545.2906, calcd 545.2897), requiring 15 degrees of unsaturation. The IR spectrum showed abundant absorption bands for the hydroxyl group (3378 cm^{-1}), carbonyl group (1734 cm^{-1}), and phenyl ring (1606, 1513, and 1446 cm^{-1}). The ^{13}C NMR spectrum of **1** showed 18

Received: August 24, 2013
Published: November 12, 2013

   dx.doi.org/10.1021/jo401859u | J. Org. Chem. 2013, 78, 11835–11848

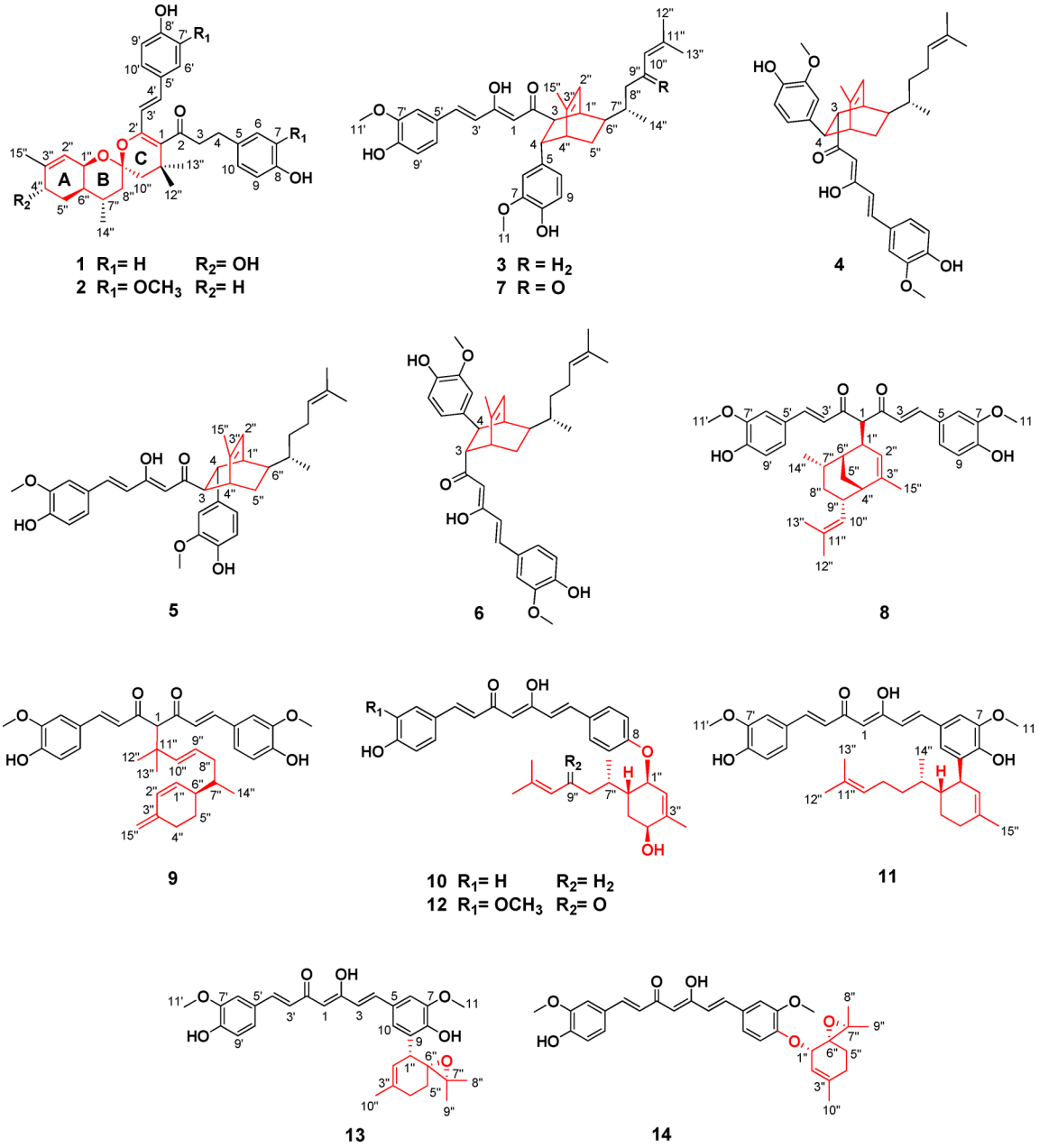

Figure 1. Structures of terpecurcumins J–W (**1**–**14**) isolated from *Curcuma longa* L.

sp^2 resonances (12 of which were assigned to two A_2B_2 aromatic rings), a ketone signal (δ_C 206.8), and a characteristic quaternary signal (δ_C 98.0) for a doubly oxygenated carbon (Table 1). The remaining unsaturations in compound **1** should be due to three rings. $^1H-^1H$ COSY, HSQC, and HMBC spectral analysis for **1** indicated the presence of three substructures **1a** (from 4″-OH to C-1 and C-2′), **1b** (from C-3′ to 8′-OH), and **1c** (from C-2 to 8-OH) (Supporting Information Figure S1). Substructure **1a** was established by starting from an oxygenated cyclohexene ring with a methyl substituent, which was characterized by the HMBC correlations of H_3-15″/C-2″, C-3″, and C-4″, H-2″/C-4″ and C-6″, and H_2-5″/C-1″ and C-4″. The HMBC correlations of H_3-14″/C-6″, C-7″, C-8″, and C-9″ and of H-8″/C-9″, as well as the $^1H-^1H$ COSY correlations of H-6″/H-7″/H-8″ and H_3-14″/H-7″, established the linkage of C-6″ and C-7″, the latter of which was further connected to C-8″ and C-9″. The methyl signals at δ_H 1.10 (H_3-12″) and 1.32 (H_3-13″) exhibited long-range correlations with C-10″, C-11″, and C-1. This evidence suggested the quaternary carbon (C-11″), which bears two methyl groups, was situated between C-10″ and C-1. In addition, the HMBC correlations of H_3-12″/C-9″, H_3-13″/C-9″ and C-2′, and H-10″/C-9″ indicated the connection of C-9″ to C-2′. The chemical shifts for C-2′ (δ_C 146.5) and C-1″ (δ_C 73.0) (Table 2), as well as the HMBC correlation of H-8″/C-2′, suggested that the spiroketal carbon C-9″ (δ_C 98.0) was simultaneously linked to C-1″ and C-2 through ether bonds and thus established the substructure **1a** containing a hydrobenzannulated[6,6]-spiroketal core. The substructure **1b** was established by the $^1H-^1H$ COSY correlations of H-3′/H-4′, H-6′/H-7′, and H-9′/H-10′, as well as the HMBC correlations of H-6′ and H-10′ with C-8′ and C-4′ and of H-3′ with C-5′. Substructures **1a** and **1b** were connected through C-2′–C-3′, according to the HMBC correlations of H-4′ with

dx.doi.org/10.1021/jo401859u | J. Org. Chem. 2013, 78, 11835–11848

Table 1. ^{1}H NMR Data for Terpecurcumins J−P (1−7) in Acetone-d_6 Recorded at 600 MHz (δ in ppm, J in Hz)

no.	1	2	3	4	5	6	7
1			5.73 (s)	5.88 (s)	5.69 (s)	5.85 (s)	5.72 (s)
3	3.03 (m, 2H)	3.01 (m, 2H)	2.96 (d, 6.5)	2.75 (dd, 6.4, 2.2)	3.02 (d, 7.6)	2.69 (m)	2.94 (d, 6.0)
4	2.91 (m, 2H)	2.90 (m, 2H)	3.13 (d, 6.5)	3.38 (d, 6.4)	3.07 (dd, 7.6, 1.7)	3.35 (d, 6.0)	3.13 (d, 6.0)
6	7.11 (d, 9.0)	6.69 (d, 1.7)	6.95 (d, 1.8)	6.80 (d, 1.8)	6.97 (d, 1.5)	6.77 (d, 2.4)	6.81 (m)
7	6.77 (d, 9.0)						
9	6.77 (d, 9.0)	6.71 (m)	6.80 (d, 8.2)	6.71 (d, 8.1)	6.80 (d, 8.1)	6.68 (d, 7.8)	6.81 (m)
10	7.11 (d, 9.0)	6.82 (d, 1.7)	6.82 (d, 8.2)	6.64 (dd, 8.1, 1.8)	6.82 (m)	6.62 (dd, 7.8, 2.4)	6.94 (s)
11		3.71 (s)	3.86 (s)	3.90 (s)	3.86 (s)	3.80 (s)	3.85 (s)
3′	6.14 (d, 15.6)	6.33 (d, 15.5)	6.52 (d, 15.8)	6.55 (d, 15.8)	6.52 (d, 15.8)	6.56 (d, 16.2)	6.51 (d, 16.2)
4′	6.72 (d, 15.6)	6.77 (m)	7.47 (d, 15.8)	7.50 (d, 15.8)	7.47 (d, 15.8)	7.51 (d, 16.2)	7.43 (d, 16.2)
6′	7.06 (d, 9.0)	6.78 (m)	7.27 (d, 1.5)	7.28 (d, 1.6)	7.27 (d, 1.3)	7.30 (d, 1.8)	7.26 (d, 1.2)
7′	6.80 (d, 9.0)						
9′	6.80 (d, 9.0)	6.80 (m)	6.85 (d, 8.2)	6.86 (d, 8.2)	6.85 (d, 8.2)	6.86 (d, 7.8)	6.84 (d, 8.4)
10′	7.06 (d, 9.0)	7.03 (d, 1.7)	7.11 (dd, 8.2, 1.5)	7.12 (dd, 8.2, 1.6)	7.10 (dd, 8.2, 1.5)	7.13 (dd, 7.8, 1.8)	7.09 (dd, 8.4, 1.2)
11′		3.82 (s)	3.89 (s)	3.81 (s)	3.88 (s)	3.90 (s)	3.87 (s)
1″	4.44 (d, 2.4)	4.40 (br s)	3.06 (d, 6.2)	2.99 (d, 6.5)	2.61 (d, 6.5)	2.68 (m)	2.99 (d, 6.0)
2″	5.20 (br s)	5.19 (s)	5.67 (d, 6.2)	6.06 (d, 6.5)	5.96 (d, 6.5)	5.80 (d, 6.0)	5.66 (d, 6.0)
4″	4.21 (t, 4.8)	2.08 (m)[a]	2.33 (s)	2.38 (s)	2.75 (s)	2.68 (m)	2.33 (s)
		1.70 (m)[b]					
5″	2.36 (m)[a]	2.04 (m)[a]	1.83 (m)[a]	1.88 (m)[a]	1.31 (m)[a]	1.88 (m)[a]	1.85 (m)[a]
	1.52 (m)[b]	1.59 (m)[b]	0.77 (m)[b]	0.96 (m)[b]	0.99 (m)[b]	0.86 (m)[b]	0.80 (m)[b]
6″	1.71 (m)	1.57 (m)	1.71 (m)	1.65 (m)	1.67 (m)	1.65 (m)	1.75 (m)
7″	2.29 (m)	2.36 (m)	1.13 (m)	1.10 (m)	1.08 (m)	1.10 (m)	1.68 (m)
8″	1.75 (m)[a]	1.78 (m)[a]	1.56 (m)[a]	1.43 (m)[a]	1.93 (m)[a]	1.48 (m)[a]	2.66 (dd, 15.0, 4.2)[a]
	1.29 (m)[b]	1.33 (m)[b]	1.20 (m)[b]	1.16 (m)[b]	1.04 (m)[b]	1.12 (m)[b]	2.15 (m)[b]
9″			2.09 (m)[a]	1.98 (m)[a]	1.72 (m, 2H)	2.04 (m)[a]	
			1.92 (m)[b]	1.72 (m)[b]		1.88 (m)[b]	
10″	1.75 (m)[a]	1.76 (m)[a]	5.15 (t, 7.1)	5.08 (t, 6.9)	5.00 (t, 7.0)	5.10 (t, 7.2)	6.15 (s)
	1.58 (m)[b]	1.59 (m)[b]					
12″	1.10 (s)	1.12 (s)	1.67 (s)	1.62 (s)	1.61 (s)	1.64 (s)	1.86 (s)
13″	1.32 (s)	1.32 (s)	1.63 (s)	1.57 (s)	1.47 (s)	1.59 (s)	2.10 (s)
14″	1.02 (d, 6.6)	0.98 (d, 6.5)	0.82 (d, 6.2)	0.78 (d, 6.5)	0.73 (d, 6.4)	0.80 (d, 6.6)	0.80 (d, 6.0)
15″	1.47 (br s)	1.45 (s)	1.86 (d, 1.1)	1.74 (d, 1.3)	1.81 (d, 1.1)	1.95 (d, 1.2)	1.85 (s)

[a]H was at the lower field. [b]H was at the higher field.

C-2′ and of H-3′ with C-1 and C-9″. The remaining substructure **1c** contained a *p*-hydroxybenzyl group according to the NMR data (Table 1). The HMBC correlations of H-3 with C-2, of H-4 with C-2 and C-3, and of H-6 and H-10 with C-4 indicated the connection of C-2−C-3−C-4−C-5. Substructures **1a** and **1c** were believed to connect through C-1−C-2 bond, albeit the expected HMBC correlation between H-3 and C-1 was too weak to be observed. Based on the above deductions, the planar structure of **1** was established as shown in Figure 1.

The relative configuration of **1** was determined based on NOE spectra and coupling constants of key proton signals (Figure S2). The NOE enhancements of H-1″(δ_H 4.44, d, 2.4 Hz) with H-6″ and H-5″b, of H-4″ with H-5″a, H-7″, and H_3-14″, and of H-5″a with H_3-14″ indicated that the A/B ring junction has a *cis* configuration. Thus, H-1″, H-6″, H-5″b, and 4″-OH were oriented on the same side of the A ring, while H-4″, H-5″a, H-7″, and H_3-14″ were on the other side. Likewise, the NOE enhancements of H-2″/H-7″, H-6″/H-8″b, and H-7″/H-8″a suggested that H-1″, H-6″, and H-8″b were oriented on the same side of the B ring, while H-2″, H-7″, and H-8″a were on the other side. Although the NOE enhancements of H_3-12″/H-10″b, H_3-13″/H-10″a, and H_3-13″/H-2″ were observed, configuration of the spiro junction of ring B and ring C was still unable to be established by NOE experiment due to signal overlapping of H-8″a and H-10″a.

In order to fully establish the structure of **1**, we obtained its single crystals from a methanol−water (45:55, v/v) solution after repeated attempts. X-ray diffraction experiment (Cu Kα) unambiguously confirmed the structure of **1** and determined its absolute configuration as 1″*S*,4″*S*,6″*R*,7″*S*,9″*R* (Figure 2).

Terpecurcumin K (**2**) should have a molecular formula of $C_{36}H_{44}O_7$, according to its HRESIMS spectrum ($[M + H]^+$ *m*/*z* 589.3177, calcd 589.3159). Its NMR data were similar to those of **1** except for the presence of two methoxyl signals (δ_H 3.71, 3.82), and one oxygenated methine (δ_C 66.3) in **1** was replaced by a methylene (δ_C 25.9) in **2**. The two methoxyl groups were assigned to H_3-11 (δ_H 3.71) and H_3-11″ (δ_H 3.82) according to their HMBC correlations with C-7 (δ_C 148.2) and C-7′ (δ_C 148.4), respectively. The methylene signal at δ_C 25.9 was assigned to C-4″ by the HMBC correlations of H_3-15″/C-2″, C-3″, and C-4″ and the ^{1}H−^{1}H COSY correlations of H-4″/H-5″ (Figure S3). Thus, compound **2** was a close analogue of **1**. The relative configuration of the hydrobenzannulated [6,6]-spiroketal moiety in **2** was the same as **1**. Particularly, the NOE enhancement between CH_3-13″ and H-2″ (Figure S4) indicated that the spiro junction of rings B and C in **2** had the same relative configuration as **1**. In addition, compounds **1** and **2** showed very similar ECD spectra (Figure S5), indicating that

dx.doi.org/10.1021/jo401859u | J. Org. Chem. 2013, 78, 11835−11848

Table 2. ^{13}C NMR Data for Terpecurcumins J–P (1–7) in Acetone-d_6 Recorded at 150 MHz (δ in ppm)

no.	1	2	3	4	5	6	7
1	125.2 (qC)	125.3 (qC)	100.4 (CH)	101.3 (CH)	100.2 (CH)	101.3 (CH)	100.3 (CH)
2	206.8 (qC)	206.8 (qC)	204.5 (qC)	203.7 (qC)	204.6 (qC)	204.0 (qC)	206.0 (qC)
3	50.3 (CH_2)	50.3 (CH_2)	56.2 (CH)	59.4 (CH)	52.5 (CH)	57.6 (CH)	56.4 (CH)
4	29.6 (CH_2)	30.6 (CH_2)	45.7 (CH)	43.6 (CH)	48.5 (CH)	47.0 (CH)	45.4 (CH)
5	133.4 (qC)	133.8 (qC)	135.4 (qC)	139.0 (qC)	134.7 (qC)	139.5 (qC)	135.3 (qC)
6	130.5 (CH)	121.6 (CH)	113.0 (CH)	111.8 (CH)	113.0 (CH)	112.1 (CH)	120.8 (CH)
7	116.0 (CH)	148.2 (qC)	148.3 (qC)	148.7 (qC)	148.2 (qC)	147.9 (qC)	148.2 (qC)
8	156.5 (qC)	145.6 (qC)	145.9 (qC)	149.7 (qC)	145.8 (qC)	145.6 (qC)	145.9 (qC)
9	116.0 (CH)	115.7 (CH)	115.6 (CH)	115.5 (CH)	115.5 (CH)	115.4 (CH)	115.6 (CH)
10	130.5 (CH)	112.8 (CH)	120.8 (CH)	120.6 (CH)	120.9 (CH)	120.7 (CH)	112.9 (CH)
11		56.0 (CH_3)	56.3 (CH_3)	56.2 (CH_3)	56.3 (CH_3)	56.1 (CH_3)	56.2 (CH_3)
2′	146.5 (qC)	147.4 (qC)	177.2 (qC)	176.8 (qC)	177.2 (qC)	176.9 (qC)	176.7 (qC)
3′	118.5 (CH)	119.4 (CH)	120.7 (CH)	120.6 (CH)	120.7 (CH)	120.5 (CH)	120.7 (CH)
4′	132.0 (CH)	132.5 (CH)	140.1 (CH)	140.3 (CH)	140.3 (CH)	140.3 (CH)	140.0 (CH)
5′	128.9 (qC)	129.6 (qC)	128.3 (qC)	128.2 (qC)	128.2 (qC)	128.2 (qC)	128.2 (qC)
6′	129.3 (CH)	121.1 (CH)	111.2 (CH)	111.3 (CH)	111.2 (CH)	111.2 (CH)	111.2 (CH)
7′	116.3 (CH)	148.4 (qC)	148.7 (qC)	148.1 (qC)	148.7 (qC)	148.8 (qC)	148.7 (qC)
8′	158.5 (qC)	147.9 (qC)	149.7 (qC)	145.8 (qC)	149.8 (qC)	149.8 (qC)	149.7 (qC)
9′	116.3 (CH)	116.1 (CH)	116.2 (CH)	116.2 (CH)	116.1 (CH)	116.1 (CH)	116.1 (CH)
10′	129.3 (CH)	111.1 (CH)	123.5 (CH)	123.5 (CH)	123.6 (CH)	123.6 (CH)	123.5 (CH)
11′		56.2 (CH_3)	56.3 (CH_3)	56.1 (CH_3)	56.3 (CH_3)	56.3 (CH_3)	56.2 (CH_3)
1″	73.0 (CH)	73.1 (CH)	38.3 (CH)	38.4 (CH)	41.7 (CH)	41.9 (CH)	38.4 (CH)
2″	129.3 (CH)	127.6 (CH)	122.5 (CH)	125.6 (CH)	126.7 (CH)	124.6 (CH)	122.5 (CH)
3″	136.7 (qC)	133.1 (qC)	144.9 (qC)	143.2 (qC)	141.4 (qC)	143.2 (qC)	145.1 (qC)
4″	66.3 (CH)	25.9 (CH_2)	45.0 (CH)	45.4 (CH)	41.1 (CH)	41.9 (CH)	44.9 (CH)
5″	34.5 (CH_2)	23.9 (CH_2)	26.5 (CH_2)	34.1 (CH_2)	35.2 (CH_2)	27.6 (CH_2)	26.3 (CH_2)
6″	42.6 (CH)	40.1 (CH)	46.7 (CH)	38.2 (CH)	36.7 (CH)	46.5 (CH)	46.5 (CH)
7″	23.2 (CH)	22.2 (CH)	38.6 (CH)	38.2 (CH)	38.1 (CH)	38.3 (CH)	35.7 (CH)
8″	44.8 (CH_2)	44.7 (CH_2)	35.4 (CH_2)	35.2 (CH_2)	33.4 (CH_2)	35.3 (CH_2)	50.3 (CH_2)
9″	98.0 (qC)	98.1 (qC)	25.7 (CH_2)	25.0 (CH_2)	24.9 (CH_2)	25.6 (CH_2)	200.7 (qC)
10″	48.6 (CH_2)	48.9 (CH_2)	125.9 (CH)	125.8 (CH)	125.8 (CH)	125.8 (CH)	128.2 (CH)
11″	32.4 (qC)	32.5 (qC)	131.3 (qC)	131.3 (qC)	131.3 (qC)	131.3 (qC)	154.3 (qC)
12″	31.1 (CH_3)	31.1 (CH_3)	25.9 (CH_3)	25.8 (CH_3)	25.8 (CH_3)	25.8 (CH_3)	27.4 (CH_3)
13″	29.3 (CH_3)	29.3 (CH_3)	17.9 (CH_3)	17.7 (CH_3)	17.6 (CH_3)	17.7 (CH_3)	20.4 (CH_3)
14″	19.3 (CH_3)	19.3 (CH_3)	17.2 (CH_3)	17.0 (CH_3)	17.1 (CH_3)	17.1 (CH_3)	17.9 (CH_3)
15″	20.2 (CH_3)	24.0 (CH_3)	20.0 (CH_3)	21.7 (CH_3)	21.0 (CH_3)	19.7 (CH_3)	19.9 (CH_3)

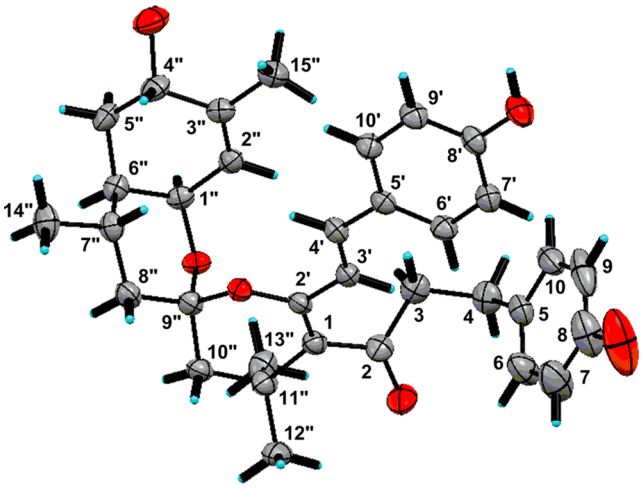

Figure 2. X-ray crystallographic structure of terpecurcumin J (1).

2 also had the absolute configuration of 1″*S*, 6″*R*, 7″*S*, and 9″*R*. In order to further confirm the absolute configuration, the ECD spectra of 1 and 2 were predicted by time-dependent density functional theory (TDDFT) calculations at the B3LYP/6-31G* level in the gas phase and in acetonitrile (MeCN) solution with the IEFPCM model. The absolute configuration of 1 predicted by ECD spectra calculations (Figure 3) gave the same result as X-ray diffraction, suggesting that ECD calculations could be used to establish the absolute configuration of similar hydrobenzannulated[6,6]-spiroketals. As shown in Figure 3, the calculated ECD spectra for 1″*S*,6″*R*,7″*S*,9″*R*-2, in contrast to 1″*R*,6″*S*,7″*R*,9″*S*-2, were similar to the experimental ECD spectrum of 2. Therefore, the absolute configuration of 2 was confirmed to be 1″*S*,6″*R*,7″*S*,9″*R*.

Terpecurcumin L (3) was obtained as orange amorphous powder. Its molecular formula $C_{36}H_{44}O_6$ was established by HRESIMS ($[M + H]^+$ m/z 573.3224, calcd 573.3211). The NMR spectra suggested 3 should be a hybrid of curcumin (moiety A) and α-zingiberene (moiety B) as illustrated in Figure S6. For moiety A, the *trans*-olefinic signals for H-3 and H-4 in curcumin were replaced by two vicinal aliphatic methine signals δ_H 3.13 (H-4, d, J = 6.5 Hz) and 2.96 (H-3, d, J = 6.5 Hz).[13] The signals for moiety B were similar to those of (−)-α-zingiberene, a major sesquiterpene previously reported from *C. longa*.[14,15] The cyclohexene ring substituted with a methyl group and an alkene chain [$(CH_3)_2C{=}CH{-}CH_2{-}CH_2{-}CH(CH_3){-}$] was established by the HMBC correlations of

dx.doi.org/10.1021/jo401859u | J. Org. Chem. 2013, 78, 11835–11848

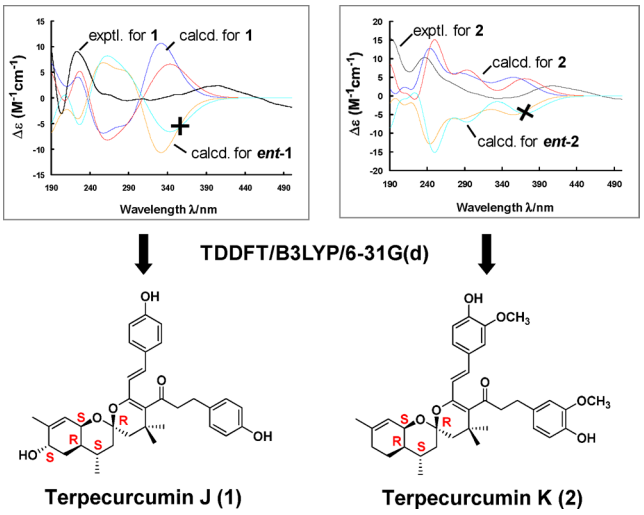

Figure 3. Comparison of the calculated ECD spectra for (1″*S*,4″*S*,6″*R*,7″*S*,9″*R*)-**1**, (1″*S*,6″*R*,7″*S*,9″*R*)-**2**, and their enantiomers (*ent*-**1** and *ent*-**2**), with the experimental ECD spectra for **1** and **2**. Experimental spectra for **1** and **2** in MeCN (black line); calculated ECD spectra for (1″*S*,4″*S*,6″*R*,7″*S*,9″*R*)-**1** and (1″*S*,6″*R*,7″*S*,9″*R*)-**2** at the B3LYP/6-31G* level in the gas phase (dark blue line) and in MeCN solution with the IEFPCM model (red line); calculated ECD spectra for *ent*-**1** and *ent*-**2** at the B3LYP/6-31G* level in the gas phase (orange line) and in MeCN solution with the IEFPCM model (light blue line)

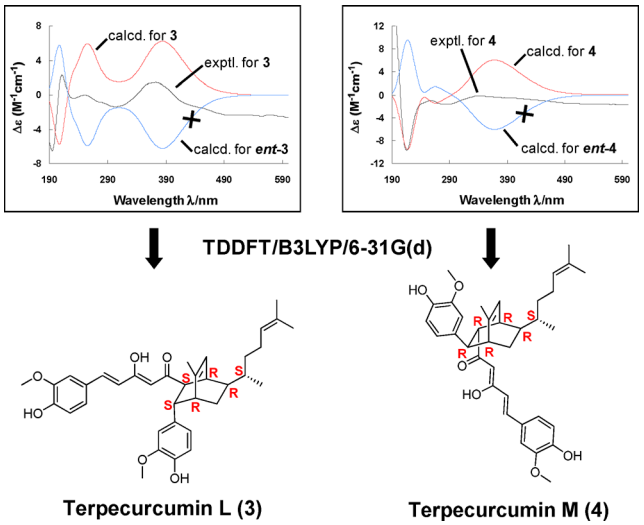

Figure 4. Comparison of the calculated ECD spectra for (3*S*,4*S*,1″*R*,4″*R*,6″*R*,7″*S*)-**3**, (3*R*,4*R*,1″*R*,4″*R*,6″*R*,7″*S*)-**4**, and their enantiomers (*ent*-**3** and *ent*-**4**), with the experimental ECD spectra for **3** and **4**. Experimental spectra for **3** and **4** in MeCN (black line); calculated ECD spectra for (3*S*,4*S*,1″*R*,4″*R*,6″*R*,7″*S*)-**3** and (3*R*,4*R*,1″*R*,4″*R*,6″*R*,7″*S*)-**4** at B3LYP/6-31G* level in MeCN solution with the IEFPCM model (red line); calculated ECD spectra for *ent*-**3** and *ent*-**4** at B3LYP/6-31G* level in MeCN solution with the IEFPCM model (blue line).

H-1″/C-3″, CH_3-15″/C-2″, C-3″, and C-4″, and CH_3-12″/C-10″, C-11″, and C-13″, as well as the ^{1}H−^{1}H COSY correlations of H-4″/H-5″/H-6″/H-1″/H-2″ and H-10″/H-9″/H-8″/H-7″/CH_3-14″. The alkene chain was connected to C-6″ of the cyclohexene ring, as evidenced by the HMBC correlations of H-8″ and CH_3-14″ with C-6″ and the ^{1}H−^{1}H COSY correlation of H-6″/H-7″ (Figure S6). The connection between moieties A and B through C-3 and C-1″ was established by the HMBC correlations of H-3/C-2″and C-6″ and H-1″/C-2, as well as the ^{1}H−^{1}H COSY correlation of H-3/H-1″. The above signals accounted for 14 of the 15 unsaturation degrees of **3** and indicated a connection between C-4 and C-4″. This connection was evidenced by the HMBC correlations of H-4/C-3″ and C-5″ and H-4″/C-3, as well as the ^{1}H−^{1}H COSY correlation of H-4/H-4″. Thus, terpecurcumin L was deduced to contain an unprecedented skeleton with a bicyclo[2.2.2]octene motif. The relative configuration of compound **3** was established by NOE experiments (Figure S7). Significant NOE enhancements of H-3/H-6, H-10, and H-6″ and H-6″/H-10 indicated that H-3, H-6″, and the benzene ring at C-4 were oriented on the same side of the cyclohexane ring. Likewise, NOE enhancements of H-4/H-15″, as well as H-2″/H-7″ and CH_3-14″, indicated that H-4, H-2″, H-15″, and the side chain at C-6″ were on the other side. The *trans*-relationship between H-3 and H-4 complied with the Alder−Stein rule.[16] From a biosynthetic point of view, compound **3** could be derived from curcumin and (−)-*α*-zingiberene via Diels−Alder [4 + 2] cycloaddition. (−)-*α*-Zingiberene is a major sesquiterpene in turmeric, and its absolute configuration had been assigned as 6″*R*,7″*S* by chemical synthesis.[17,18] Taken into consideration the established relative configuration of **3**, the ECD spectrum for (3*S*,4*S*,1″*R*,4″*R*,6″*R*,7″*S*)-**3** was calculated by TDDFT and matched the experimental data very well (Figure 4). Therefore, the absolute configuration of **3** was determined to be 3*S*,4*S*,1″*R*,4″*R*,6″*R*,7″*S*.

Compounds **4**−**6** were isomers of **3**. Their UV, IR, and NMR spectra were very similar to each other, indicating that they all contained curcumin and (−)-*α*-zingiberene units, albeit the linkage pattern may be different. For terpecurcumin M (**4**), the HMBC correlations of H-3/C-2″ and C-6″, H-4/C-3″, H-1″/C-2, and H-4″/C-3, together with the ^{1}H−^{1}H COSY correlations of H-3/H-1″ and H-4/H-4″ suggested that the two units were also linked by C3−C1″ and C4−C4″ bonds (Figure S8). The NOE enhancements of H-3/H-2″, H-6, and H-10 as well as H-2″/H-14″ revealed that H-3, H-2″, the benzene ring at C-4, and the side chain at C-6″ were oriented on the same side of the cyclohexane ring. In the meanwhile, the enhancement of H-4/H-6″ indicated that H-4 and H-6″ were on the other side (Figure S9). Thus, compounds **3** and **4** only differed in the configurations of C-3 and C-4. By comparing the predicted and experimental ECD spectra (Figure 4), the absolute configuration of **4** was determined to be 3*R*,4*R*,1″*R*,4″*R*,6″*R*,7″*S*. For terpecurcumin N (**5**), the HMBC correlations of H-3/C-3″and C-5″, H-4″/C-2, H-4/C-2″, and C-6″, and H-1″/C-3 indicated that the curcumin and (−)-*α*-zingiberene units were linked by C3−C4″ and C4−C1″ bonds (Figure S10). This linkage was further confirmed by the ^{1}H−^{1}H COSY correlations of H-3/H-4″ and H-4/H-1″. The relative configuration of **5** was determined by NOE experiments. The NOE enhancements of H-3/H-6″, H-6, and H-10 and of H-6″/H-10 suggested that H-3, H-6″, and the benzene ring at C-4 were oriented on the same side of the cyclohexane ring, whereas H-4 and H-2″ were on the other side (Figure S11). The absolute configuration of **5** was assigned as 3*R*,4*R*,1″*R*,4″*R*,6″*R*,7″*S* by comparing the calculated and experimental ECD spectra (Figure S12). Terpecurcumin O (**6**) was a diastereoisomer of **5**, according to the HMBC correlations of H-3/C-3″ and C-5″ and H-4″/C-2, as well as the ^{1}H−^{1}H COSY correlations of H-3/H-4″ and H-4/H-1″ (Figure S13). The NOE enhancements between H-3 and H-

dx.doi.org/10.1021/jo401859u | J. Org. Chem. 2013, 78, 11835−11848

Table 3. ^{1}H NMR Data for Terpecurcumins Q–W (8–14) in Acetone-d_6 Recorded at 600 MHz (δ in ppm, J in Hz)

no.	8	9	10	11	12	13	14
1	4.35 (d, 12.0)	4.43 (s)	5.99 (s)	5.97 (s)	6.01 (s)	5.96 (s)	5.99 (s)
3	6.94 (m)	6.91 (m)	6.71 (d, 16.2)	6.65 (d, 15.6)	6.72 (d, 15.6)	6.66 (d, 15.6)	6.72 (d, 15.6)
4	7.65 (dd, 16.2, 3.0)	7.56 (d, 16.0)	7.62 (d, 16.2)	7.58 (d, 15.6)	7.63 (d, 15.6)	7.59 (d, 15.6)	7.59 (d, 15.6)
6	7.33 (br s)	7.30 (s)	7.64 (m)	7.19 (s)	7.64 (m)	7.25 (s)	7.31 (s)
7			7.00 (d, 8.4)		7.02 (d, 8.4)		
9	6.87 (m)	6.88 (m)	7.00 (d, 8.4)		7.02 (d, 8.4)		7.15 (m)
10	7.21 (m)	7.19 (d, 8.0)	7.64 (m)	7.02 (s)	7.64 (m)	7.18 (s)	7.19 (m)
11	3.89 (s)	3.90 (s)		3.92 (s)		3.89 (s)	3.89 (s)
3′	6.94 (m)	6.91 (m)	6.66 (d, 16.2)	6.68 (d, 15.6)	6.73 (d, 16.2)	6.69 (d, 15.6)	6.73 (d, 15.6)
4′	7.65 (dd, 16.2, 3.0)	7.56 (d, 16.0)	7.61 (d, 16.2)	7.58 (d, 15.6)	7.62 (m)	7.58 (d, 15.6)	7.61 (d, 15.6)
6′	7.33 (br s)	7.30 (s)	7.56 (d, 8.4)	7.30 (s)	7.35 (s)	7.32 (s)	7.34 (s)
7′			6.90 (d, 8.4)				
9′	6.87 (m)	6.88 (m)	6.90 (d, 8.4)	6.88 (d, 8.4)	6.89 (d, 8.4)	6.87 (d, 8.4)	6.89 (d, 7.8)
10′	7.21 (m)	7.19 (d, 8.0)	7.56 (d, 8.4)	7.16 (d, 8.4)	7.19 (dd, 8.4, 1.2)	7.16 (d, 8.4)	7.17 (m)
11′	3.89 (s)	3.90 (s)		3.90 (s)	3.93 (s)	3.91 (s)	3.93 (s)
1″	3.18 (m)	5.61 (d, 10.0)	4.76 (d, 9.0)	3.85 (d, 9.6)	4.78 (d, 9.0)	3.90 (m)	4.61 (d, 4.8)
2″	5.40 (br s)	6.11 (d, 10.0)	5.54 (s)	5.19 (s)	5.53 (s)	5.40 (d, 4.8)	5.78 (d, 4.8)
4″	2.07 (m)	2.36 (m)[a]	4.01 (s)	2.07 (m)[a]	4.03 (s)	2.26 (m, 2H)	2.26 (m)[a]
		2.23 (m)[b]		2.00 (m)[b]			1.53 (m)[b]
5″	1.84 (m)[a]	1.65 (m, 2H)	1.80 (m)[a]	1.73 (m)[a]	1.85 (m)[a]	2.16 (m)[a]	2.60 (m)[a]
	1.54 (m)[b]		1.56 (m)[b]	1.42 (m)[b]	1.62 (m)[b]	1.44 (m)[b]	1.53 (m)[b]
6″	1.40 (br s)	2.20 (m)	2.22 (m)	1.72 (m)	2.14 (m)		
7″	1.63 (m)	1.58 (m)	1.91 (m)	1.40 (m)	2.47 (m)		
8″	1.25 (m)[a]	2.09 (m)[a]	1.37 (m)[a]	1.30 (m)[a]	2.47 (m)[a]	1.56 (s)	1.36 (s)
	1.03 (m)[b]	1.91 (m)[b]	1.28 (m)[b]	1.20 (m)[b]	2.36 (m)[b]		
9″	2.51 (m)	5.41 (m)	2.02 (m, 2H)	1.82 (m, 2H)		1.37 (s)	1.36 (s)
10″	4.85 (d, 9.6)	5.84 (d, 15.6)	5.12 (t, 6.6)	4.89 (t, 7.2)	6.15 (s)	1.83 (s)	1.77 (s)
12″	1.63 (s)	2.06 (s)	1.65 (m)	1.52 (s)	1.85 (s)		
13″	1.63 (s)	2.06 (s)	1.59 (m)	1.46 (s)	2.08 (s)		
14″	0.95 (d, 7.2)	0.78 (d, 6.7)	0.80 (d, 7.2)	0.85 (d, 6.6)	0.83 (d, 7.2)		
15″	1.60 (s)	4.71 (d, 8.5, 2H)	1.78 (m)	1.68 (s)	1.79 (s)		

[a]H was at the lower field. [b]H was at the higher field.

15″, H-3 and H-6, as well as H-3 and H-10 indicated that H-3, H-15″, and the benzene ring at C-4 were oriented on the same side of the cyclohexane ring. In accordance, the enhancement between H-4 and H-6″ revealed they were oriented on the other side (Figure S14). Thus, compounds **5** and **6** only differed in the configurations of C-3 and C-4. The absolute configuration of **6** was assigned as 3*S*,4*S*,1″*R*,4″*R*,6″*R*,7″*S* by comparing the predicted and experimental ECD spectra (Figure S12).

Terpecurcumin P (**7**) is an oxygenated analogue of **3**. Its NMR spectra showed a carbonyl signal at δ_C 200.7, which was assigned to C-9″ according to the HMBC correlations of H-8″ and H-10″/C-9″ (Figure S15). In accordance, C-8″ ($\Delta\delta_C$ +15.0) and C-11″ ($\Delta\delta_C$ +23.0) shifted downfield remarkably when compared to **3** (Table 2). The NOE enhancements of H-3/H-6″, H-6, and H-10 as well as H-4/H-15″ suggested that **7** had the same relative configuration as **3** (Figure S16). The absolute configuration of **7** was determined to be 3*S*,4*S*,1″*R*,4″*R*,6″*R*,7″*S* by ECD spectra calculation (Figure S12).

Terpecurcumin Q (**8**) was obtained as orange amorphous powder. Its molecular formula $C_{36}H_{42}O_6$ was established by HRESIMS ([M + H]$^+$ m/z 571.3059, calcd 571.3054), indicating 16 degrees of unsaturation. The NMR spectra (Tables 3 and 4) suggested that **8** should be a hybrid of a curcumin unit (moiety A) and a sesquiterpene unit (moiety B), as illustrated in Figure S17. Moiety B was proven to be an unusual sesquiterpene skeleton with a bicyclo[3.1.3]octene core substituted by two methyl groups and one isobutenyl group. DEPT experiment revealed that moiety B consisted of four methyls at δ_C 26.6, 26.6, 20.0, and 17.8, two methylenes at δ_C 35.1 and 32.1, seven methines at δ_C 130.7, 126.3, 41.4, 40.3, 37.4, 36.1, and 35.4, and two quaternary carbons at δ_C 138.0 and 130.3. The bicyclo[3.1.3]octene core was established by the HMBC correlations of H-1″/C-2″ and C-3″, H-2″/C-4″ and C-6″, H-5″/C-7″ and C-9″, and H-8″/C-4″, as well as ^{1}H–^{1}H COSY correlations of H-1″/H-2″ and H-4″/H-5″/H-6″/H-7″/H-8″/H-9″ (Figure S17). The isobutenyl group was established by the HMBC correlations of H-10″/C-12″and C-13″, together with CH_3-12″/C-11″ and C-13″. The substitution position of CH_3-15″, CH_3-14″, and the isobutenyl group was assigned to C-3″, C-7″, and C-9″, respectively. These deductions were supported by the HMBC correlations of CH_3-15″/C-2″, C-3″, and C-4″, CH_3-14″/C-7″ and C-8″, and H-10″/C-8″ and C-9″, as well as ^{1}H–^{1}H COSY correlations of CH_3-14″/H-7″ and H-10″/H-9″. The linkage of moieties A and B was determined to be a C–C bond between C-1 and C-1″ according to the HMBC correlation of H-1/C-1″, as well as the ^{1}H–^{1}H COSY correlation of H-1/H-1″ (Figure S17). The above deductions established the planar structure of **8**. The bicyclo[3.1.3]octene core is formed by C-4/9 linkage of a bisabolane skeleton. This unusual sesquiterpene unit was connected to C-1 of curcumin. This was different from the

dx.doi.org/10.1021/jo401859u | J. Org. Chem. 2013, 78, 11835–11848

Table 4. ^{13}C NMR Data for Terpecurcumins Q–W (8–14) in Acetone-d_6 Recorded at 150 MHz (δ in ppm)

no.	8	9	10	11	12	13	14
1	70.2 (CH)	72.2 (CH)	101.8 (CH)	101.3 (CH)	101.8 (CH)	101.5 (CH)	101.7 (CH)
2	194.7 (qC)	195.0 (qC)	184.1 (qC)	184.7 (qC)	184.1 (qC)	184.6 (qC)	184.1 (qC)
3	123.7 (CH)	125.3 (CH)	122.6 (CH)	121.9 (CH)	122.7 (CH)	122.1 (CH)	122.3 (CH)
4	145.0 (CH)	143.7 (CH)	140.6 (CH)	141.9 (CH)	140.6 (CH)	141.8 (CH)	141.0 (qC)
5	127.4 (qC)	127.6 (qC)	128.5 (qC)	127.3 (qC)	128.6 (qC)	127.0 (qC)	128.1 (qC)
6	111.8 (CH)	111.9 (CH)	130.9 (CH)	108.0 (CH)	130.9 (CH)	109.5 (CH)	112.2 (CH)
7	148.7 (qC)	148.7 (qC)	116.7 (CH)	148.2 (qC)	116.8 (CH)	149.4 (qC)	151.6 (qC)
8	150.6 (qC)	150.4 (qC)	161.2 (qC)	147.9 (qC)	161.0 (qC)	148.6 (qC)	151.6 (qC)
9	116.2 (CH)	116.2 (CH)	116.7 (CH)	133.0 (qC)	116.8 (CH)	129.6 (qC)	117.7 (CH)
10	124.6 (CH)	124.2 (CH)	130.9 (CH)	123.6 (CH)	130.9 (CH)	123.8 (CH)	123.2 (CH)
11	56.3 (CH_3)	56.3 (CH_3)		56.3 (CH_3)		56.4 (CH_3)	56.3 (CH_3)
2′	194.5 (qC)	195.0 (qC)	184.8 (qC)	184.1 (qC)	184.8 (qC)	184.3 (qC)	183.6 (qC)
3′	123.5 (CH)	125.3 (CH)	122.0 (CH)	122.2 (CH)	122.2 (CH)	122.3 (CH)	122.9 (CH)
4′	145.0 (CH)	143.7 (CH)	141.1 (CH)	141.1 (CH)	141.5 (CH)	141.2 (CH)	141.5 (CH)
5′	127.4 (qC)	127.6 (qC)	127.6 (qC)	128.1 (qC)	128.1 (qC)	128.1 (CH)	129.5 (qC)
6′	111.7 (CH)	111.9 (CH)	130.9 (CH)	111.4 (CH)	111.5 (CH)	111.5 (CH)	111.5 (CH)
7′	148.7 (qC)	148.7 (qC)	116.7 (CH)	148.7 (qC)	148.8 (qC)	148.7 (qC)	148.8 (qC)
8′	150.6 (qC)	150.4 (qC)	160.5 (qC)	149.9 (qC)	150.1 (qC)	149.9 (qC)	150.0 (qC)
9′	116.2 (CH)	116.2 (CH)	116.7 (CH)	116.1 (CH)	116.2 (CH)	116.2 (CH)	116.2 (CH)
10′	124.5 (CH)	124.2 (CH)	130.9 (CH)	123.9 (CH)	123.9 (CH)	123.7 (CH)	123.8 (CH)
11′	56.3 (CH_3)	56.3 (CH_3)		56.2 (CH_3)	56.3 (CH_3)	56.3 (CH_3)	56.3 (CH_3)
1″	35.4 (CH)	135.7 (CH)	75.9 (CH)	38.5 (CH)	75.7 (CH)	37.8 (CH)	74.9 (CH)
2″	126.3 (CH)	130.3 (CH)	124.5 (CH)	126.5 (CH)	124.2 (CH)	122.8 (CH)	120.8 (CH)
3″	138.0 (qC)	144.5 (qC)	140.1 (qC)	134.5 (qC)	140.3 (qC)	137.3 (qC)	143.2 (qC)
4″	40.3 (CH)	30.8 (CH_2)	67.5 (CH)	31.1 (CH_2)	67.4 (CH)	31.0 (CH_2)	31.4 (CH_2)
5″	32.1 (CH_2)	24.8 (CH_2)	30.8 (CH_2)	22.9 (CH_2)	31.6 (CH_2)	24.4 (CH_2)	23.6 (CH_2)
6″	36.1 (CH)	40.5 (CH)	38.1 (CH)	44.5 (CH)	39.2 (CH)	69.2 (qC)	67.1 (qC)
7″	37.4 (CH)	38.2 (CH)	31.2 (CH)	32.8 (CH)	28.9 (CH)	64.3 (qC)	61.8 (qC)
8″	35.1 (CH_2)	38.2 (CH_2)	35.7 (CH_2)	36.2 (CH_2)	49.7 (CH_2)	21.3 (CH_3)	21.2 (CH_3)
9″	41.4 (CH)	126.8 (CH)	26.5 (CH_2)	26.5 (CH_2)	200.1 (qC)	20.5 (CH_3)	20.8 (CH_3)
10″	130.7 (CH)	140.4 (CH)	125.5 (CH)	125.4 (CH)	124.9 (CH)	23.4 (CH_3)	23.4 (CH_3)
11″	130.3 (qC)	40.5 (qC)	131.5 (qC)	131.2 (qC)	154.5 (qC)		
12″	26.6 (CH_3)	26.8 (CH_3)[a]	25.8 (CH_3)	25.7 (CH_3)	27.4 (CH_3)		
13″	17.8 (CH_3)	26.5 (CH_3)[a]	17.7 (CH_3)	17.6 (CH_3)	20.5 (CH_3)		
14″	20.0 (CH_3)	16.1 (CH_3)	15.1 (CH_3)	15.1 (CH_3)	15.4 (CH_3)		
15″	26.6 (CH_3)	110.3 (CH_2)	20.8 (CH_3)	23.6 (CH_3)	20.7 (CH_3)		

[a]Values may be interchanged.

previously reported terpecurcumins A–I, where the sesquiterpene unit was substituted at C-9 or 8-OH of curcumin.[10]

The relative configuration of **8** was determined by NOE experiments (Figure S18). The enhancements of H-1″/H-2″, H-8″b, and CH_3-14″ and H-9″/H-4″ and H-5″b indicated that H-1″, H-2″, H-8″b, and CH_3-14″ possessed the same orientation, while H-4″, H-5″b, H-6″, H-7″, and H-9″ were in the opposite orientation. The absolute configuration of **8** was determined to be 1″*R*,4″*S*,6″*R*,7″*S*,9″*S*, by comparing the experimental ECD spectrum with TDDFT calculated ECD spectra (Figure 5). Molecular orbital (MO) analysis of conformer **8-48** (Figure 6) suggested that the positive Cotton effect at ca. 206 nm mainly originated from the electronic transitions MO141→LUMO154 and MO144→MO155 of the sesquiterpene substructure involving $\sigma\rightarrow\pi^*$ and $\pi\rightarrow\pi^*$ transitions, while the $\pi\rightarrow\pi^*$ transitions in the curcumin unit from MO143 and MO147 to LUMO154 may contribute to the weak Cotton effects at 230–450 nm. We calculated the ECD spectra of a truncated model of **8** (**TM8**, Figure 5) and obtained the same absolute configuration for the sesquiterpene unit as described above. Given that the computational workload for the truncated model was much lower than the whole molecule of **8**, this strategy will be used to determine the absolute configuration of compound **9**.

Terpecurcumin R (**9**) is an isomer of **8**, as deduced from HRESIMS spectrum ($[M + H]^+$ *m*/*z* 571.3059, calcd 571.3054). The NMR spectra indicated that compound **9** also possessed a curcumin unit (moiety A) (Tables 3 and 4). The remaining part (moiety B) was deduced to be a sesquiterpene similar to (−)-β-sesquiphellandrene or (+)-β-turmerone.[19] A cyclohexene ring bearing an exocyclic double bond and a side chain $(CH_3)_2C{-}CH{=}CH{-}CH_2{-}CH(CH_3){-}$ was established by HMBC and $^1H{-}^1H$ COSY correlations (Figure S19). The HMBC correlations of H-1/C-10″, C-12″, and C-13″, CH_3-12″/C-1, and CH_3-13″/C-1 suggested that moieties A and B were connected through C-1 and C-11″. Based on the above deductions, the planar structure of **9** was established as shown in Figure 1. Given the flexible structure of compound **9**, particularly the curcumin moiety, to calculate its ECD spectra by TDDFT was time-consuming. Based on our experience with compound **8**, calculating the spectra for the sesquiterpene moiety could obtain the same result while the computation workload could be remarkably reduced. Thus, ECD spectra of a truncated model of **9** (**TM9**)

dx.doi.org/10.1021/jo401859u | J. Org. Chem. 2013, 78, 11835–11848

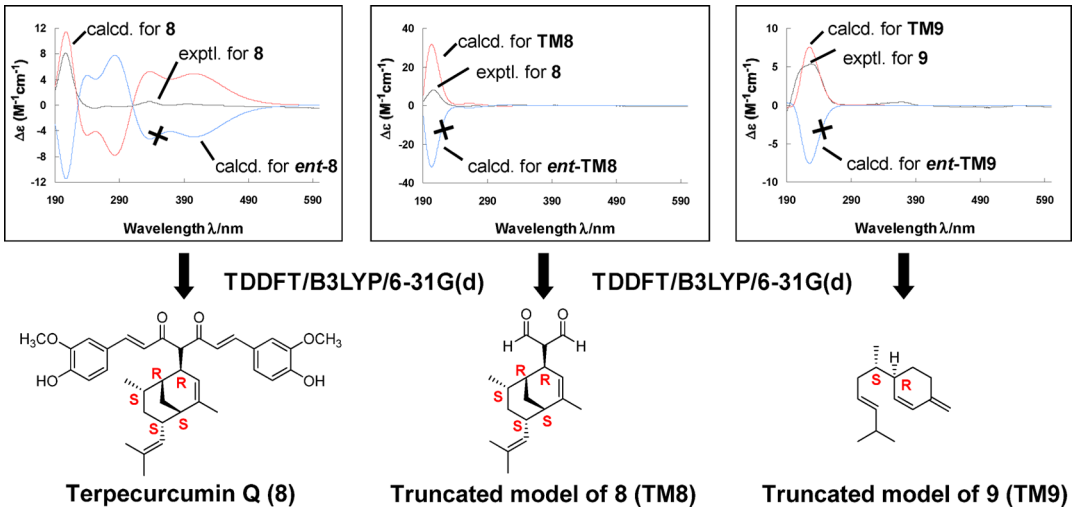

Figure 5. Comparison of the calculated ECD spectra for (1″*R*,4″*S*,6″*R*,7″*S*,9″*S*)-**8**, the truncated models of (1″*R*,4″*S*,6″*R*,7″*S*,9″*S*)-**8** (**TM8**) and (6″*R*,7″*S*)-**9** (**TM9**), and their enantiomers (*ent*-**8**, *ent*-**TM8**, and *ent*-**TM9**), with the experimental ECD spectra for **8** and **9**. Experimental spectra for **8** and **9** in MeCN (black line); calculated ECD spectra for (1″*R*,4″*S*,6″*R*,7″*S*,9″*S*)-**8**, **TM8**, and **TM9** at the B3LYP/6-31G* level in MeCN solution with the IEFPCM model (red line); calculated ECD spectra for *ent*-**8**, *ent*-**TM8**, and *ent*-**TM9** at the B3LYP/6-31G* level in MeCN solution with the IEFPCM model (blue line).

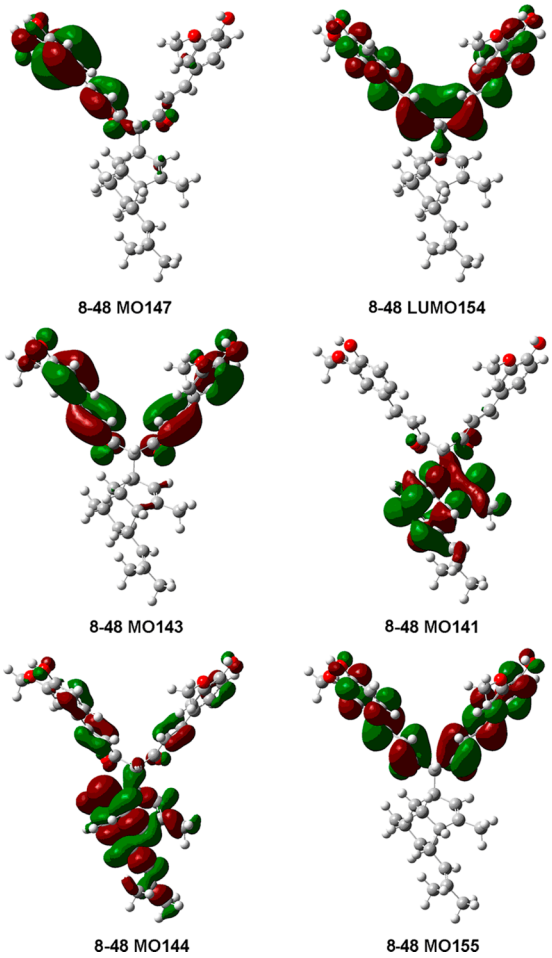

Figure 6. Important molecular orbitals (MO) involved in the key transitions in ECD spectrum of conformer **8-48** in MeCN with IEFPCM model at the B3LYP/6-31G(d) level.

were predicted. In the 200−250 nm region, the calculated ECD spectra for **TM9** (6″*R*,7″*S*) showed similar positive Cotton effects to the experimental spectrum for compound **9** and thus determined its absolute configuration as 6″*R*,7″*S* (Figure 5). Furthermore, we isolated from turmeric a major compound (+)-*β*-turmerone (6″*R*, 7″*S*), a close analogue of the sesquiterpene moiety of **9** (Figure S20).[20,21] The experimental ECD spectrum of (+)-*β*-turmerone was very similar to that of **9**, exhibiting a positive Cotton effect at 240 nm ($\Delta\varepsilon$ +6.94) (Figure S21). This result also indicated that compound **9** possessed the absolute configuration of 6″*R*,7″*S*.

Terpecurcumin S (**10**) was deduced to have a molecular formula of $C_{34}H_{40}O_5$, $C_2H_4O_2$ less than that of terpecurcumin A.[10] The ^{1}H NMR spectrum of **10** displayed no methoxyl signal, and the two aromatic ABX systems in terpecurcumin A were replaced by an A_2B_2 system in **10** (Table 3), which were further confirmed by HMBC and ^{1}H−^{1}H COSY (Figure S22). Thus, compound **10** contained a bisdemethoxycurcumin unit instead of curcumin. The sesquiterpene structure of **10** was the same as that of terpecurcumin A, according to their similar NMR data (Figure S23). Their similar ECD spectra suggested that they had the same absolute configuration (Figure S24). The absolute configuration of terpecurcumin A had been determined in our previous report by ECD spectral calculations.[10] Here we used vibrational circular dichroism (VCD) calculation to verify the ECD results. As shown in Figure 7, the VCD spectrum calculated for (1″*R*,4″*S*,6″*R*,7″*S*) rather than (1″*S*,4″*R*,6″*S*,7″*R*) showed much similarity with the experimental VCD spectrum for terpecurcumin A and thus confirmed the absolute configuration of terpecurcumin A as 1″*R*,4″*S*,6″*R*,7″*S*. The VCD calculation results showed a confidence level of 94%, and the ESI value of 45.7 lies at the 35th percentile in the database for correct assignments (Figure S25).[22] The results suggested that both ECD and VCD calculations could predict the absolute configuration of terpecurcumins accurately, in spite of their flexible structures. Based on the above evidence, the absolute configuration of **10** was established as 1″*R*,4″*S*,6″*R*,7″*S*.

Terpecurcumin T (**11**) has the molecular formula $C_{36}H_{44}O_6$, as established by HRESIMS. Its NMR spectra were very similar to the previously reported terpecurcumin I,[10] except that C-9″

dx.doi.org/10.1021/jo401859u | J. Org. Chem. 2013, 78, 11835−11848

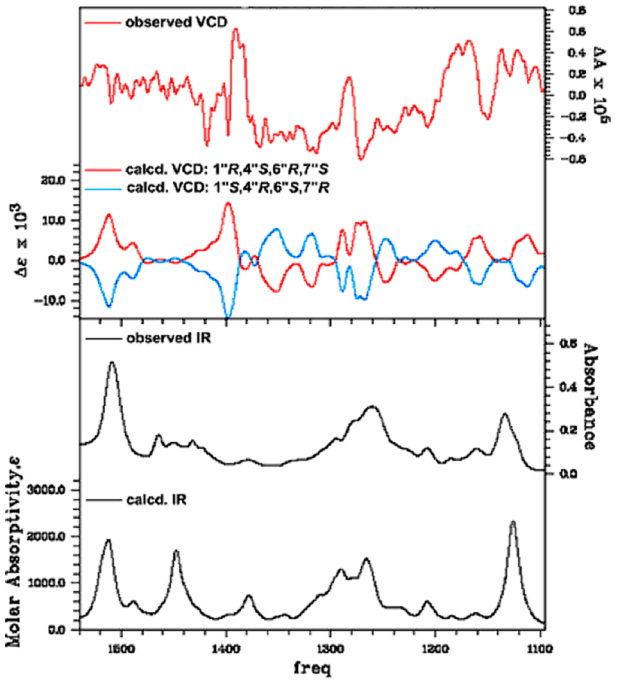

Figure 7. Comparison of the experimental VCD spectrum for terpecurcumin A with calculated VCD spectra for its possible enantiomers (1″*R*,4″*S*,6″*R*,7″*S*) and (1″*S*,4″*R*,6″*S*,7″*R*).

in **11** was a methylene (δ_C 26.5) instead of a carbonyl group (δ_C, 200.4) (Tables 3 and 4). This was supported by the triplet of H-10″ (singlet for terpecurcumin I), the upfield shifts of C-8″ ($\Delta\delta_C$ −14.8) and C-11″ ($\Delta\delta_C$ −23.1), and ^{1}H−^{1}H COSY correlations of H-8″/H-9″/H-10″ in **11** (Figure S26). The large *trans*-diaxial coupling constant (J_{aa} = 9.6 Hz) suggested a *trans* relationship between H-1″ and H-6″. Considering that compound **11** had very similar planar structure with terpecurcumin I and that their ECD spectra showed much similarity (Figure S24), the absolute configuration of **11** was assigned as 1″*R*,6″*R*,7″*S*.

Terpecurcumin U (**12**) showed NMR signals for demethoxycurcumin and bisacurone units and was an isomer of demethoxybisabolocurcumin ether (DMBCE) (Tables 3 and 4).[10] The main difference between **12** and DMBCE was the location of the methoxyl group (C-7′ for **12** and C-7 for DMBCE), which was established by the HMBC correlations of H-1″/C-8 and CH_3-11′/C-7′ as well as the ^{1}H−^{1}H COSY correlations of H-6/H-7 and H-9/H-10 (Figure S27). The NOE enhancements of H-1″/H-5″b, H-4″/H-5″b, and H-6″/H-5″a suggested that **12** had the same relative configuration as DMBCE (Figure S28). Their similar ECD spectra established the absolute configuration of **12** as 1″*R*,4″*S*,6″*R*,7″*S* (Figure S24).

Terpecurcumin V (**13**) has the molecular formula $C_{31}H_{34}O_7$, as established by HRESIMS spectrum ([M + H]$^+$ *m*/*z* 519.2374, calcd 519.2377). The IR spectrum indicated the existence of hydroxyl group (3422 cm^{-1}), carbonyl group (1756 cm^{-1}), phenyl ring (1626, 1599, 1509, and 1454 cm^{-1}), and oxirane ring (964 and 843 cm^{-1}).[23] The NMR spectra (Tables 3 and 4) suggested that **13** should be a hybrid of a curcumin unit (moiety A) and a terpinolene oxide unit (moiety B, a monoterpene), as illustrated in Figure S29.[24,25] Moiety B displayed a methine signal at δ_H 3.90 (m, 1H, H-1″), an olefinic signal at δ_H 5.40 (d, 1H, H-2″), two groups of methylene signals [δ_H 2.26 (m, 2H, H-4″); 2.16 and 1.44 (m, 1H each, H-5″)], and three methyl signals [δ_H 1.56 (s, 3H, H-8″), 1.37 (s, 3H, H-9″), and 1.83 (s, 3H, H-10″)]. Their connections were established by the HMBC correlations of H-1″/C-3″and C-7″, H-5″/C-6″ and C-7″, CH_3-8″/C-6″, C-7″, and C-9″, and CH_3-10″/C-2″and C-4″, as well as ^{1}H−^{1}H COSY correlations of H-1″/H-2″ and H-4″/H-5″. Moieties A and B should be linked through a C−C bond between C-9 and C-1″, as evidenced by the HMBC correlations of H-1″/C-9, H-1″/C-10, and H-10/C-1″. Although the relative configuration of **13** could not be determined by NOE experiment due to the peculiar spiroepoxide structure, the two methyl signals (δ_H 1.56 and 1.37) corresponding to the *gem*-dimethyl groups at the oxide ring could be distinguished by NOE enhancements of H-1″/H-8″ and H-5″b/H-9″ (Figure S30). The above deductions established the planar structure of **13**, which has an unprecedented skeleton conjugating curcumin with a terpinolene oxide unit through a C−C bond.

The absolute configuration of compound **13** was determined by compulational calculations of ECD spectra and ^{13}C NMR spectra. Bearing two chiral carbons (C-1″ and C-6″), compound **13** could have four possible stereoisomers [**13a** (1″*R*,6″*R*), **13b** (1″*S*,6″*S*), **13c** (1″*R*,6″*S*), and **13d** (1″*S*,6″*R*)]. The calculated ECD spectra for **13a** and **13c**, rather than **13b** or **13d**, showed much similarity with the experimental spectrum after a UV correction of 28 nm (Figure 8). To determine the

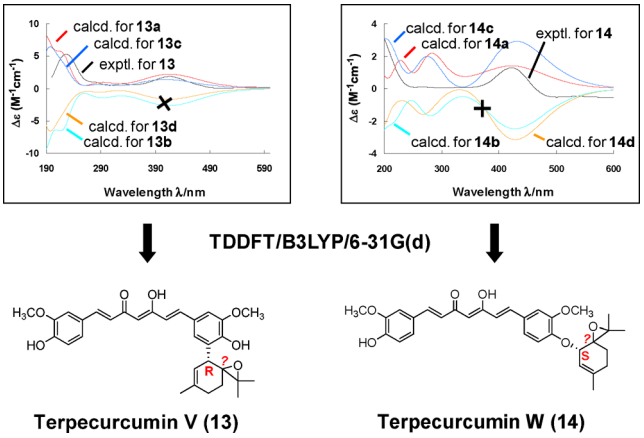

Figure 8. Comparison of the experimental ECD spectra for **13** and **14** in MeCN with those calculated for their possible stereoisomers after a UV correction of 28 nm.

absolute configuration of C-6″, we computed the ^{13}C NMR spectra for **13a** and **13c** at the B3LYP/6-311+G(2d,p)//HF/6-31G(d) level.[26] The calculation was particularly focused on the carbon atoms of the terpinolene oxide unit because this is the region likely to be influenced by the stereochemistry of the epoxy ring. Moreover, we performed the data evaluation by considering the correlation factors R^2 (derived from a linear regression analysis of the calculated vs experimental ^{13}C chemical shifts), the absolute errors ($|\Delta\delta| = |\delta_{exp} - \delta_{calcd}|$), and the mean absolute error (MAE = $\Sigma[|\delta_{exp} - \delta_{calcd}|]/n$), which have been successfully used in the relative configuration determination of natural products.[27,28] According to Table 5, the higher R^2 (0.9982) and lower MAE (1.4 ppm) suggested **13a** as the most possible structure for **13**. Moreover, the $|\Delta\delta|$ values demonstrated that **13a** matched the experimental data better for all carbon signals than **13c**. Based on the above

dx.doi.org/10.1021/jo401859u | J. Org. Chem. 2013, 78, 11835−11848

Table 5. Linear Regression Analysis (R^2), Absolute Error ($|\Delta\delta|$), and Mean Absolute Error (MAE) for the Calculated ^{13}C Chemical Shifts of 13a, 13c, 14a, and 14c versus the Experimental Values of 13 and 14

no.	δ_{calcd} (13a)	δ_{calcd} (13c)	δ_{exp} (13)	$\lvert\Delta\delta\rvert_{calcd}$ (13a)	$\lvert\Delta\delta\rvert_{calcd}$ (13c)	δ_{calcd} (14a)	δ_{calcd} (14c)	δ_{exp} (14)	$\lvert\Delta\delta\rvert_{calcd}$ (14a)	$\lvert\Delta\delta\rvert_{calcd}$ (14c)
1″	39.7	43.2	37.8	1.9	5.4	74.6	71.8	74.9	0.3	3.1
2″	122.6	124.0	122.8	0.2	1.2	120.0	116.3	120.8	0.8	4.5
3″	139.3	138.5	137.3	2.0	1.2	144.2	148.6	143.2	1.0	5.4
4″	32.6	28.8	31	1.6	2.2	32.6	30.8	31.4	1.2	0.6
5″	25.9	28.1	24.4	1.5	3.7	24.9	25.1	23.6	1.3	1.5
6″	66.1	64.8	69.2	3.1	4.4	66.7	64.9	67.1	0.4	2.2
7″	61.7	61.4	64.3	2.6	2.9	61.2	62.8	61.8	0.6	1.0
8″	21.1	19.7	21.3	0.2	1.6	20.9	20.5	21.2	0.3	0.7
9″	19.7	20.0	20.5	0.8	0.5	19.4	22.0	20.8	1.4	1.2
10″	23.3	23.6	23.4	0.1	0.2	23.7	25.1	23.4	0.3	1.7
R^2	0.9982	0.9952				0.9996	0.9959			
MAE				1.4	2.3				0.8	2.2

Scheme 1. Plausible Biosynthetic Pathway for Terpecurcumins J (1) and K (2)

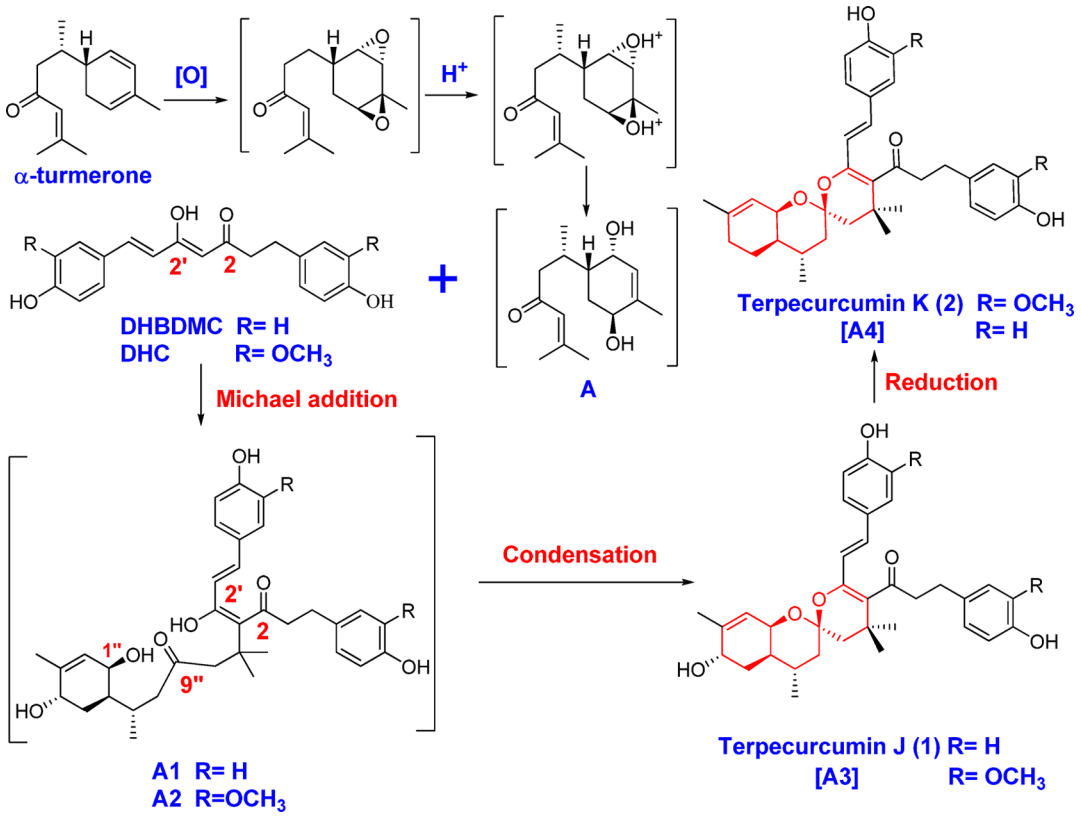

evidence, the absolute configuration of **13** was finally established as **13a** (1″*R*,6″*R*).

Terpecurcumin W (**14**) is an isomer of **13**. The NMR spectral data indicated that **14** also possessed the curcumin and terpinolene oxide units (Tables 3 and 4). The only difference was the linkage pattern. The HMBC correlation of H-1″/C-8 in compound **14** suggested these two units were connected through C-8−O−C-1″ rather than the C-9−C-1″ bond. This deduction was confirmed by the upfield shift of C-9 ($\Delta\delta$ −11.9) and the downfield shift of C-1″ ($\Delta\delta$ +37.1). In accordance, H-9 resonated at δ_H 7.15, which showed HMBC correlations with C-5 (δ_C 129.5) and C-7 (δ_C 151.6) (Figure S31). The NOE enhancement of H-1″/H-9 suggested a *cis* configuration between H-1″ and C-8 (Figure S32). Similar to compound **13**, the absolute configuration of **14** was determined by ECD and ^{13}C NMR spectra calculations. As shown in Figure 8, the calculated ECD spectra for **14a** (1″*S*,6″*S*) and **14c** (1″*S*,6″*R*) were consistent with the experimental spectrum for **14** and thus determined the absolute configuration of C-1″ as *S*. The ^{13}C NMR spectra for **14a** and **14c** were then predicted. As shown in Table 5, **14a** showed higher R^2 value (0.9996 vs 0.9959) and lower MAE value (0.8 vs 2.2) than **14c**. Therefore, the absolute configuration of **14** was established as 1″*S*,6″*R*.

Plausible Biosynthetic Origin of Terpecurcumins J−W (1−14). Terpecurcumins J−W (**1**−**14**) constituted a novel class of natural products conjugating the diarylheptanoid skeleton with a sesqui- or monoterpene. Among them, terpecurcumins J−Q (**1**−**8**) and V (**13**) represented four unprecedented skeletons featuring an unusual core of hydrobenzannulated[6,6]-spiroketal (**1** and **2**), bicyclo[2.2.2]octane (**3**−**7**), bicyclo[3.1.3]octane (**8**), and spiroepoxide (**13**), respectively. Their novel structures prompted us to speculate

dx.doi.org/10.1021/jo401859u | J. Org. Chem. 2013, 78, 11835−11848

their biosynthetic pathways, particularly correlations between the new skeletons with known turmeric compounds.

The hydrobenzannulated[6,6]-spiroketal core is very rare in natural products. Terpecurcumins J (**1**) and K (**2**) are the first hydrobenzannulated[6,6]-spiroketals isolated from higher plants. More importantly, the novel carbon skeleton is derived from hybridization of a diarylheptanoid and a sesquiterpene unit and represents a distinct biosynthetic pathway from the recently reported sponge sesterterpenes containing a similar core.[29−31] Therefore, terpecurcumins J (**1**) and K (**2**) have significant novelty not only in the carbon skeleton but also in the biogenetic origin. They could be derived from α-turmerone and dihydrobisdemethoxycurcumin (DHBDMC)/dihydrocurcumin (DHC) through oxidation, ring opening, Michael addition, and condensation reactions, as depicted in Scheme 1. Initially, α-turmerone could be oxidized and followed by opening of the epoxy ring to produce **A**. Subsequent Michael addition may hybridize **A** with DHBDMC and DHC to produce **A1** and **A2**, respectively, which further undergo a key condensation reaction to yield terpecurcumin J (**1**) and **A3**. Finally, terpecurcumin J (**1**) and **A3** could be reduced to generate **A4** and terpecurcumin K (**2**), respectively. This speculation was supported by LC/MS/MS analysis of turmeric. The key biosynthetic intermediates **A3** and **A4** could be detected, though in trace amounts, in the rhizomes of *C. longa* (Figure S33).

Terpecurcumins L−P (**3**−**7**) represent an unprecedented skeleton containing a bicyclo[2.2.2]octene motif resulted from the conjugation of curcumin and a sesquiterpene units via Diels−Alder [4 + 2] cycloaddition (Scheme 2). Interestingly,

Scheme 2. Plausible Biosynthetic Pathway for Terpecurcumins L−P (3−7)

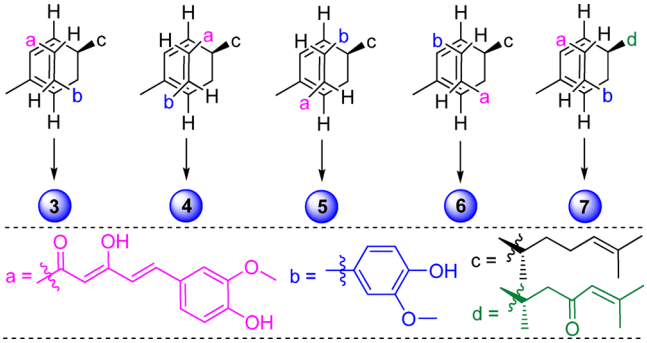

compounds **3**−**6** represent all the four possible stereoisomers. Their structures only differ in the linkage pattern of the two units. For compounds **3** and **4**, the two units were linked through C-3−C-1″ and C-4−C-4″ bonds. The same units were linked through C-3−C-4″ and C-4−C-1″ bonds for compounds **5** and **6**. Diels−Alder addition has been extensively reported in natural products.[32,33] Recently, Liu et al. isolated an enzyme which could catalyze Diels−Alder cycloaddition from a microbial strain.[34] The enzymes responsible for the non-stereoselective biosynthesis of **3**−**7** in *Curcuma longa* warrants future study.

Terpecurcumins Q (**8**) and R (**9**) feature a sesquiterpene unit connected to C-1 of curcumin. Particularly, terpecurcumin Q (**8**) contains an unprecedented carbon skeleton bearing an unusual bicyclo[3.1.3]octene core formed by C-4″/9″ linking of a bisabolane skeleton. The biosynthetic precursor of **8** could be traced back to (−)-α-zingiberene, which was abundant in the volatile oil of turmeric (Figure S34). (−)-α-Zingiberene could be oxidized, rearranged, and then cyclized (undergoing dehydration) to produce a carbocation, which could then hybridize with the curcumin anion to produce **8**. Likewise, compound **9** could be derived from another abundant compound in turmeric oil, (−)-β-sesquiphellandrene (Figure S35).

Terpecurcumins S−U (**10**−**12**) should have similar biosynthetic pathways with the previously reported terpecurcumins A−I.[10] The bisabolane units could be derived from α-turmerone/zingiberene, which undertake oxidative rearrangements, and then conjugate to curcuminoid anion by electrophilic substitution (Figure S36). Terpecurcumins V (**13**) and W (**14**) represent the first examples of monoterpene-conjugated curcuminoids. They could also be biosynthesized by electrophilic substitution of curcumin with an α-terpineol-derived carbocation (Figure S37).[25]

Terpecurcumins J−W (**1**−**14**) are curcuminoids hybridized with sesqui- or monoterpenes through different linkage patterns. Given their fairly low amounts in *Curcuma longa*, whether these compounds are genuine natural products needs to be proved. To this end, turmeric powder was directly analyzed by MALDI-TOF-MS without sample extraction. Majority of the terpecurcumins could be detected, although the pseudomolecular ion peaks were very low in the mass spectra (Figure S38). Furthermore, we macerated turmeric powder in 95% ethanol at room temperature for 5 min and then analyzed the sample by LC/MS rapidly. A number of terpecurcumins could be clearly detected and were identified by comparing with reference compounds (Figure S39). These experiments proved that terpecurcumins J−W were true secondary metabolites of *Curcuma longa*, instead of artifacts formed during extraction and separation.

Cytotoxic Activity Evaluation of Terpecurcumins. The overall growth inhibitory effects of terpecurcumins J−W (**1**−**14**) were evaluated against human breast cancer cells (MDA-MB-231 and MCF-7), human liver cancer cells (HepG2), and human lung cancer cells (A549) using crystal violet staining method as previously described.[35] Paclitaxel was used as the positive control, which showed IC_{50} values of 0.039−0.062 μM. Compounds **8** and **9** showed significant cytotoxicities with IC_{50} values of 3.9−12.3 μM for all the four cell lines (Table S1). The other compounds were inactive (IC_{50}, 11.8−60.5 μM), while most terpecurcumins showed more potent cytotoxicities than curcumin (IC_{50}, 31.7−49.5 μM) and ar-/β-turmerone (>100 μM). It was particularly noteworthy that compound **8** showed IC_{50} of 3.9 μM against MCF-7 cells. Morphologic observations of terpecurcumin-treated MCF-7 cells suggested that induction of apoptosis contributed to the overall growth inhibition. PI single staining demonstrated that compounds **3**, **7**, and **8** did not perturb the cell cycle but increased the sub-G1 peaks corresponding to apoptotic cells (Figure S40). Exposure of 5 and 7.5 μM terpecurcumin Q (**8**) for 48 h increased the percentage of sub-G1 cells from 2.03% of control to 26.35 and 28.55%, respectively, which were remarkably higher than curcumin (2.95% for 5 μM and 1.86% for 7.5 μM). Accordingly, cleaved PARP (polyADP-ribosepolymerase) bands, as a result of caspase digestion, could be clearly observed in Western blotting analysis of compounds **3**, **7**, and **8** treated MCF-7 cells. This result suggested that caspase activation may play an important role in the apoptosis induction of terpecurcumins. To elucidate whether the caspase

dx.doi.org/10.1021/jo401859u | J. Org. Chem. 2013, 78, 11835−11848

activation is mediated by the mitochondrial pathway, mitochondria-associated proteins were analyzed by Western blotting. Although terpecurcumin Q (**8**) at 5 μM showed little effect on the pro-apoptotic protein Bax, it could induce the expression of Bak and significantly suppress the antiapoptotic proteins Bcl-2 and Bcl-xl. This phenomenon was not observed in the same concentration of curcumin. Taken together, terpecurcumin Q showed potential for the treatment of breast cancer, albeit the mechanism warrants further evaluation.

Quantitative Analysis of Representative Terpecurcumins. Terpecurcumins J (**1**) and P (**7**) could be the minor unknown curcuminoids with molecular weights of 544 and 586 Da discovered by Ourisson and co-workers in 1980. However, these compounds were not isolated and identified from *C. longa* at that time due to low abundance.[36] To further understand the abundance of these novel terpene-conjugated curcuminoids in turmeric, a rapid and sensitive LC/MS/MS method was established to simultaneously determine five terpecurcumins **1**, **3**, **7**, **8**, and **13**, which represented different carbon skeletons (Figure S41). The mass spectrometer was monitored in the selected reaction monitoring (SRM) mode, and all five analytes showed good linearity (r > 0.9914) (Table S2). The terpecurcumins were detected in all 14 batches of turmeric at parts per million level (generally below 40 μg/g, Table S3). Among them, compounds **1**, **3**, and **8** showed very low abundance with an average of 3.50, 4.45, and 2.41 ppm, respectively. The contents may be closely related to the abundance of their biosynthetic precursors. Due to the low abundance of bisdihydrodemethoxycurcumin in turmeric, compound **1** had a small amount ranging from 0.42 to 6.68 ppm. In addition, contents of the five terpecurcumins varied significantly among different batches. For instance, the content of terpecurcumin V (**13**) was 146.96 and 134.72 ppm in batches 7 and 13, respectively, and was only 2.73 ppm in batch 8. It is also noteworthy that samples collected from Sichuan Province, which is a long-time major cultivation area for *C. longa* in China and is generally considered to produce high-quality turmeric (also called authentic crude drugs in China), did not contain significantly higher amounts of terpecurcumins than the other samples.

EXPERIMENTAL SECTION

Plant Material, Extraction, and Isolation. The 1 year old rhizomes of *Curcuma longa* L. were collected from Pengzhou City, Sichuan Province, China, in December 2009. Identification of the plant was performed by one of the authors (M. Ye). A voucher specimen (No. JH200912) was deposited at School of Pharmaceutical Sciences, Peking University, Beijing, China. Powder of the air-dried rhizomes (30 kg) was extracted with 95% aq EtOH at 80 °C two times (1 h each time). The extract was concentrated under reduced pressure to afford a residue, which was purified over MCI gel eluted with 80% MeOH to remove the major curcuminoids including curcumin, demethoxycurcumin, and bisdemethoxycurcumin. The sample was then eluted with MeOH to obtain a concentrated extract (291 g), which was separated by silica gel column chromatography ($CHCl_3$/MeOH, 100:0 to 2:1, v/v) to obtain nine fractions (A–I) based on TLC analysis. Fraction E (20 g) was chromatographed over silica gel (1.0 kg, 200–300 mesh) and eluted with petroleum ether/EtOAc (1:0 to 2:1) to give seven fractions (EA–EG). Fraction EC (5.18 g) was purified on an ODS C_{18} column eluted with MeOH/H_2O (50 to 100%, v/v) to obtain six subfractions (ECA–ECF). ECC was further purified over Sephadex LH-20 and semipreparative HPLC (YMC Pack ODS-A, 5 μm, 250 × 10 mm i.d., MeCN/H_2O = 70:30, v/v) to yield terpecurcumins J (**1**, 9.0 mg) and K (**2**, 6.0 mg). Likewise, subfractions ECD and ECE were purified by Sephadex LH-20 column chromatography and semipreparative HPLC (MeCN/H_2O = 85:15, v/v) to obtain terpecurcumins L (**3**, 23.3 mg), M (**4**, 5.1 mg), N (**5**, 11.3 mg), O (**6**, 7.2 mg), P (**7**, 29.3 mg), S (**10**, 11.0 mg), and T (**11**, 20.0 mg). Fraction ED (3.74 g) was separated on an ODS C_{18} column eluted with MeOH/H_2O (50 to 90%, v/v) to obtain three subfractions (EDA–EDB). EDB was chromatographed over Sephadex LH-20 and then purified by semipreparative HPLC (MeCN/H_2O = 70:30, v/v) to obtain terpecurcumins Q (**8**, 13.0 mg) and R (**9**, 5.0 mg). Fraction EF (3.15 g) was purified on an ODS C_{18} column eluted with MeOH/H_2O (50 to 90%, v/v) to yield three subfractions (EFA–EFC). EFB (965.8 mg) was subjected to Sephadex LH-20 column chromatography eluted with MeOH to afford eight fractions (EFBA–EFBH). EFBC was purified by semipreparative HPLC with MeCN–H_2O (75:25, v/v) as the mobile phase to yield terpecurcumins U (**12**, 17.0 mg), V (**13**, 17.0 mg), and W (**14**, 3.6 mg). HRESIMS analysis of the pure compounds was conducted on a FT-MS instrument.

*Terpecurcumin J (**1**):* pale yellow crystals, mp 202–204 °C; $[\alpha]_D^{23}$ +2.0 (c 0.08, MeCN); UV (MeCN) λ_{max} (log ε) = 283 (3.95), 324 (4.11) nm; ECD (MeCN) λ_{max} ($\Delta\varepsilon$) = 190 (+9.78), 224 (+8.97), 400 (+2.32) nm; IR ν_{max} = 3378, 2954, 2927, 1734, 1707, 1677, 1606, 1513, 1446, 1374, 1263, 1245, 1204, 1044, 825 cm^{-1}; for ^{1}H and ^{13}C NMR data, see Tables 1 and 2; HRESIMS m/z 545.2906 [M + H]$^+$, calcd for $C_{34}H_{41}O_6$, 545.2897.

*Terpecurcumin K (**2**):* pale yellow amorphous powder; $[\alpha]_D^{23}$ +1.25 (c 0.08, MeCN); UV (MeCN) λ_{max} (log ε) = 282 (3.99), 327 (4.13) nm; ECD (MeCN) λ_{max} ($\Delta\varepsilon$) = 190 (+15.38), 236 (+10.67), 402 (+2.67) nm; IR ν_{max} = 3421, 2956, 1769, 1598, 1514, 1450, 1373, 1242, 1034, 812 cm^{-1}; for ^{1}H and ^{13}C NMR data, see Tables 1 and 2; HRESIMS m/z 589.3177 [M + H]$^+$, calcd for $C_{36}H_{45}O_7$, 589.3159.

*Terpecurcumin L (**3**):* orange amorphous powder; $[\alpha]_D^{21}$ +130 (c 0.08, MeCN); UV (MeCN) λ_{max} (log ε) = 367 (4.25) nm; ECD (MeCN) λ_{max} ($\Delta\varepsilon$) = 197 (−6.28), 212 (+2.29), 405 (+2.72) nm; IR ν_{max} = 3419, 2958, 2929, 1769, 1734, 1634, 1577, 1513, 1429, 1374, 1243, 1124, 1034, 969, 813 cm^{-1}; for ^{1}H and ^{13}C NMR data, see Tables 1 and 2; HRESIMS m/z 573.3224 [M + H]$^+$, calcd for $C_{36}H_{45}O_6$, 573.3211.

*Terpecurcumin M (**4**):* orange amorphous powder; $[\alpha]_D^{22}$ −20 (c 0.04, MeCN); UV (MeCN) λ_{max} (log ε) = 367 (4.20) nm; ECD (MeCN) λ_{max} ($\Delta\varepsilon$) = 190 (+17.32), 218 (−9.45) nm; IR ν_{max} = 3422, 2959, 2924, 1769, 1734, 1634, 1574, 1512, 1430, 1374, 1242, 1123, 1034, 965, 813 cm^{-1}; for ^{1}H and ^{13}C NMR data, see Tables 1 and 2; HRESIMS m/z 573.3219 [M + H]$^+$, calcd for $C_{36}H_{45}O_6$, 573.3211.

*Terpecurcumin N (**5**):* orange amorphous powder; $[\alpha]_D^{22}$ −27 (c 0.02, MeCN); UV (MeCN) λ_{max} (log ε) = 368 (4.17) nm; ECD (MeCN) λ_{max} ($\Delta\varepsilon$) = 201 (+11.19), 231 (+0.27) nm; IR ν_{max} = 3432, 2961, 2926, 1769, 1735, 1633, 1580, 1513, 1429, 1374, 1243, 1126, 1035, 968, 816 cm^{-1}; for ^{1}H and ^{13}C NMR data, see Tables 1 and 2; HRESIMS m/z 573.3228 [M + H]$^+$, calcd for $C_{36}H_{45}O_6$, 573.3211.

*Terpecurcumin O (**6**):* orange amorphous powder; $[\alpha]_D^{23}$ +60 (c 0.04, MeCN); UV (MeCN) λ_{max} (log ε) = 366 (3.40) nm; ECD (MeCN) λ_{max} ($\Delta\varepsilon$) = 190 (−9.86), 212 (+7.60) nm; IR ν_{max} = 3410, 2961, 2925, 1734, 1632, 1585, 1513, 1430, 1374, 1262, 1243, 1130, 1037, 968, 815 cm^{-1}; for ^{1}H and ^{13}C NMR data, see Tables 1 and 2; HRESIMS m/z 573.3226 [M + H]$^+$, calcd for $C_{36}H_{45}O_6$, 573.3211.

*Terpecurcumin P (**7**):* orange amorphous powder; $[\alpha]_D^{23}$ +183 (c 0.10, MeCN); UV (MeCN) λ_{max} (log ε) = 365 (4.32) nm; ECD (MeCN) λ_{max} ($\Delta\varepsilon$) = 200 (−10.69), 212 (+5.43), 247 (+2.32), 365 (+4.43) nm; IR ν_{max} = 3425, 2933, 1678, 1633, 1588, 1513, 1429, 1377, 1270, 1210, 1125, 1033, 970, 816, 756 cm^{-1}; for ^{1}H and ^{13}C NMR data, see Tables 1 and 2; HRESIMS m/z 587.3007 [M + H]$^+$, calcd for $C_{36}H_{43}O_7$, 587.3003.

*Terpecurcumin Q (**8**):* orange amorphous powder; $[\alpha]_D^{25}$ +99 (c 0.02, MeCN); UV (MeCN) λ_{max} (log ε) = 344 (4.26) nm; ECD (MeCN) λ_{max} ($\Delta\varepsilon$) = 206 (+8.16) nm; IR (KBr) ν_{max} = 3395, 2969, 2914, 1658, 1579, 1512, 1450, 1429, 1378, 1272, 1161, 1125, 1032, 982, 756 cm^{-1}; for ^{1}H and ^{13}C NMR data, see Tables 3 and 4; HRESIMS m/z 571.3059 [M + H]$^+$, calcd for $C_{36}H_{43}O_6$, 571.3054.

*Terpecurcumin R (**9**):* orange amorphous powder; $[\alpha]_D^{25}$ +166 (c 0.03, MeCN); UV (MeCN) λ_{max} (log ε) = 233 (4.39), 349 (4.35) nm; ECD (MeCN) λ_{max} ($\Delta\varepsilon$) = 227 (+5.39) nm; IR (KBr) ν_{max} = 3416,

2957, 2925, 1655, 1579, 1512, 1455, 1429, 1379, 1274, 1163, 1124, 1074, 1031, 980, 771 cm^{-1}; for ^1H and ^{13}C NMR data, see Tables 3 and 4; HRESIMS m/z 571.3059 $[M + H]^+$, calcd for $C_{36}H_{43}O_6$, 571.3054.

*Terpecurcumin S (**10**):* orange amorphous powder; $[\alpha]_D^{25}$ +142 (c 0.02, MeCN); UV (MeCN) λ_{max} (log ε) = 413 (4.28) nm; ECD (MeCN) λ_{max} ($\Delta\varepsilon$) = 200 (+2.98), 403 (+0.34) nm; IR (KBr) ν_{max} = 3364, 2961, 2918, 2849, 1735, 1626, 1599, 1509, 1443, 1247, 1169, 1137, 978, 831 cm^{-1}; for ^1H and ^{13}C NMR data, see Tables 3 and 4; HRESIMS m/z 529.2943 $[M + H]^+$, calcd for $C_{34}H_{41}O_5$, 529.2948.

*Terpecurcumin T (**11**):* orange amorphous powder; $[\alpha]_D^{25}$ +200 (c 0.02, MeCN); UV (MeCN) λ_{max} (log ε) = 420 (4.43) nm; ECD (MeCN) λ_{max} ($\Delta\varepsilon$) = 202 (+4.15), 405 (+0.79) nm; IR (KBr) ν_{max} = 3523, 3427, 2961, 2922, 2854, 1734, 1624, 1592, 1512, 1427, 1294, 1267, 1134, 968, 845 cm^{-1}; for ^1H and ^{13}C NMR data, see Tables 3 and 4; HRESIMS m/z 573.3219 $[M + H]^+$, calcd for $C_{36}H_{45}O_6$, 573.3211.

*Terpecurcumin U (**12**):* orange amorphous powder; $[\alpha]_D^{25}$ +170 (c 0.02, MeCN); UV (MeCN) λ_{max} (log ε) = 415 (4.37) nm; ECD (MeCN) λ_{max} ($\Delta\varepsilon$) = 200 (+3.87), 406 (+0.33) nm; IR (KBr) ν_{max} = 3409, 2962, 2935, 1734, 1623, 1597, 1509, 1445, 1246, 1134, 978, 828 cm^{-1}; for ^1H and ^{13}C NMR data, see Tables 3 and 4; HRESIMS m/z 573.2851 $[M + H]^+$, calcd for $C_{35}H_{41}O_7$, 573.2846.

*Terpecurcumin V (**13**):* orange amorphous powder; $[\alpha]_D^{25}$ +20.0 (c 0.01, MeOH); UV (MeOH) λ_{max} (log ε) = 202 (4.65), 260 (4.23), 422 (4.76) nm; ECD (MeCN) λ_{max} ($\Delta\varepsilon$) = 226 (+5.27), 419 (+1.78) nm; IR (KBr) ν_{max} = 3422, 2923, 1756, 1627, 1599, 1509, 1455, 1279, 1116, 964, 843, 611 cm^{-1}; for ^1H and ^{13}C NMR data, see Tables 3 and 4; HRESIMS m/z 519.2374 $[M + H]^+$, calcd for $C_{31}H_{35}O_7$, 519.2377.

*Terpecurcumin W (**14**):* orange amorphous powder; $[\alpha]_D^{25}$ +10.2 (c 0.02, MeOH); UV (MeOH) λ_{max} (log ε) = 202 (4.77), 259 (4.28), 419 (4.09) nm; ECD (MeCN) λ_{max} ($\Delta\varepsilon$) = 200 (+4.09), 422 (+1.70) nm; IR (KBr) ν_{max} = 3424, 2888, 1758, 1629, 1465, 1344, 1279, 1189, 1112, 963, 843, 529 cm^{-1}; for ^1H and ^{13}C NMR data, see Tables 3 and 4; HRESIMS m/z 519.2383 $[M + H]^+$, calcd for $C_{31}H_{35}O_7$, 519.2377.

X-ray Crystal Data for Terpecurcumin J (1): $C_{68}H_{79}O_{12}$ (M = 1088.31), monoclinic, space group $P2_1$ (no. 4), a = 9.3544(2) Å, b = 28.8050(7) Å, c = 11.3634(3) Å, β = 92.382(2)°, V = 3059.27(13) Å^3, Z = 2, T = 180.00(10) K, μ(Cu Kα) = 0.642 mm^{-1}, D_{calcd} = 1.181 g/mm^3, 11 980 reflections measured ($6.14 \le 2\theta \le 144.2$), 8519 unique ($R_{int}$ = 0.0295) which were used in all calculations. The final R_1 was 0.0581 (>2 $\sigma(I)$) and wR_2 was 0.1663 (all data). The goodness of fit on F^2 was 1.037. Flack parameter = 0.09 (19). Using Olex2, the crystal structure was solved with the XS structure solution program using Direct Methods and refined with the XL refinement package using Least Squares minimization. The CIF file of X-ray data for **1** has been deposited in the Cambridge Crystallographic Data Centre (deposition no. CCDC 934684).

ECD Calculations. A preliminary conformational search was performed in SYBYL-X 1.1 using random search method with the MMFF94 force field.[37] Conformers within 6 kcal/mol were saved and further optimized using the density functional theory (DFT) method at the B3LYP/6-31G* level. Frequency was calculated at the same level of theory. The stable conformers with populations greater than 1% and without imaginary frequencies were submitted to ECD calculation by the TDDFT [B3LYP/6-31G*] method. The excitation energies (E), oscillator strength (f), rotatory strength in velocity form (R_{vel}), and rotatory strength in length form (R_{len}) of the lowest 30 excited states were calculated. Considering solvent effects on calculation, we used the IEFPCM model in MeCN. ECD spectra of different conformers were simulated using SpecDis[38] with a half-bandwidth of 0.3 eV for compounds **1** and **2** and of 0.4 eV for other compounds. The final ECD spectra were generated according to the Boltzmann-calculated distribution of each conformer. The calculated ECD spectra were compared with the experimental data. All calculations were performed with Gaussian 09 program package.[39]

VCD Calculations. A conformational search was carried out with ComputeVOA[40] at the molecular mechanics level. Geometry, frequency, IR, and VCD intensity calculations were carried out at the DFT/B3LYP/6-31G* level with Gaussian 09. The calculated frequencies were scaled by 0.97, and the IR and VCD intensities were converted to Lorentzian bands with 6 cm^{-1} half-width for comparison to experiment. In order to accurately compare calculated and experimental IR and VCD data, the recently developed confidence level algorithm CompareVOA[22] was used. It allows a direct quantitative comparison of experimental and calculated spectra to provide a measure of agreement. It also provides the enantiomeric similarity index (ESI) for a given configuration and the position of this value within an internal database for correct VCD assignments.

^{13}C NMR Chemical Shift Calculations. The conformers consistent with the NOE experimental data for diastereoisomers **13a** and **13c** were optimized by using the Hartree−Fock (HF) method at the 6-31G(d) level. The stable conformers with populations greater than or equal to 1% and without imaginary frequencies were used as inputs for the ^{13}C NMR spectra calculations performed in Me_2CO employing the B3LYP function combined with the 6-311+G(2d,p) basis set. The calculated values of ^{13}C chemical shifts for **13a** and **13c** were referenced to tetramethylsilane computed at the same level of theory. The ^{13}C chemical shifts of **14a** and **14c** were calculated following similar procedures.

Cytotoxic Activity Evaluation. The overall growth inhibitory effect of terpecurcumins J−W (**1**−**14**) was evaluated against human breast cancer cells (MDA-MB-231 and MCF-7), human liver cancer cells (HepG2), and human lung cancer cells (A549) using crystal violet staining method as previously described.[35] For cell cycle analysis, MCF-7 cells were treated with terpecurcumins L−P (**3**−**7**) at 25 μM or terpecurcumin Q (**8**) at 5 and 7.5 μM for 48 h and were then harvested for sub-G1 assay. Cells were washed two times with PBS and fixed with 75% ethanol at −20 °C for 24 h. The cells were resuspended in PBS containing RNaseA (1 mg/mL), incubated for 1 h at 37 °C, and then stained with propidium iodide (PI) (10 μg/mL) for 30 min at room temperature in the dark. The DNA contents of the stained cells were analyzed using ModFit LT software with FACSCalibur flow cytometry, and sub-G1 content stands for populations of cell apoptosis. For Western blotting analysis of mitochondrial-associated proteins and cleaved PARP, the cell lysate was prepared in ice-cold radioimmunoprecipitation assay (RIPA) buffer. Cell lysates were resolved by electrophoresis and transferred to a PVDF membrane. The blot was then probed with primary antibody followed by incubation with appropriate horseradish peroxidase-conjugated secondary antibodies. The signal was visualized by enhanced chemiluminescence and recorded on an X-ray film.

LC/MS/MS Quantitative Analysis. Crude materials of *C. longa* (14 commercial batches collected from different areas in China, including no. JH200912) was powdered and sifted (80 mesh). An aliquot of 2.0 g was mixed with 10 mL of methanol. The mixture was vortexed (2200 rpm) for 1 min and then ultrasonicated (150 W, 40 kHz) in a water bath at 30 °C for 60 min. The supernatant was passed through a 0.22 μm filter, and an aliquot of 10 μL was injected for LC/MS/MS analysis. Compounds **1**, **3**, **7**, **8**, and **13** were separated on a reversed-phase HPLC column, eluted with a gradient of acetonitrile/water/formic acid (Figure S41), and then detected using a triple quadrupole mass spectrometer in (−)-SRM mode. The working solutions were prepared by serially diluting a stock solution of mixed standards (0.006, 0.018, 0.06, 0.18, 0.6, 1.8, 6, and 18 μg/mL for each compound). Regression equations were established by plotting the peak areas (duplicate injections) against nominal concentrations (Table S2).

■ ASSOCIATED CONTENT

Ⓢ Supporting Information

Key HMBC and $^1H-^1H$ COSY correlations, NOE enhancements, 1D and 2D NMR, IR and HRESIMS spectra for compounds **1**−**14**; crystal cell diagram and CIF file for **1**; and cytotoxicity evaluation and Western blotting analysis data. This material is available free of charge via the Internet at http://pubs.acs.org.

AUTHOR INFORMATION

Corresponding Author

*Tel/Fax: +86 10 82802024. E-mail: yemin@bjmu.edu.cn.

Notes

The authors declare no competing financial interest.

ACKNOWLEDGMENTS

This work was supported by National Natural Science Foundation of China (No. 81222054), the Program for New Century Excellent Talents in University from Chinese Ministry of Education (No. NCET-11-0019), and China State Administration of TCM (No. 201307002). We wish to thank Prof. Laurence A. Nafie (Department of Chemistry, Syracuse University/BioTools, Inc., USA) for the VCD measurement and calculation, and Dr. N.D. Wang (College of Chemistry and Molecular Engineering, Peking University) for his kind help with crystal structure analysis.

REFERENCES

(1) Jemal, A.; Bray, F.; Center, M. M.; Ferlay, J.; Ward, E.; Forman, D. *Ca-Cancer J. Clin.* **2011**, *61*, 69−90.

(2) Printz, C. *Cancer* **2012**, *118*, 289−291.

(3) Chabner, B. A. *N. Engl. J. Med.* **2011**, *365*, 2147−2149.

(4) Newman, D. J.; Cragg, G. M. *J. Nat. Prod.* **2012**, *75*, 311−335.

(5) Li, R.; Xiang, C.; Zhang, X.; Guo, D. A.; Ye, M. *Curr. Pharm. Anal.* **2010**, *6*, 256−268.

(6) Li, S.; Yuan, W.; Deng, G.; Wang, P.; Yang, P.; Aggarwal, B. B. *Pharm. Crops* **2011**, *2*, 28−54.

(7) Esatbeyoglu, T.; Huebbe, P.; Ernst, I. M.; Chin, D.; Wagner, A. E.; Rimbach, G. *Angew. Chem., Int. Ed.* **2012**, *51*, 5308−5332.

(8) Gupta, S. C.; Prasad, S.; Kim, J. H.; Patchva, S.; Webb, L. J.; Priyadarsinic, I. K.; Aggarwal, B. B. *Nat. Prod. Rep.* **2011**, *28*, 1937−1955.

(9) Teiten, M. H.; Gaigneaux, A.; Chateauvieux, S.; Billing, A. M.; Planchon, S.; Fack, F.; Renaut, J.; Mack, F.; Muller, C. P.; Dicato, M.; Diederich, M. *OMICS* **2012**, *16*, 289−300.

(10) Lin, X. H.; Ji, S.; Li, R.; Dong, Y. H.; Qiao, X.; Hu, H. B.; Yang, W. Z.; Guo, D. A.; Tu, P. F.; Ye, M. *J. Nat. Prod.* **2012**, *75*, 2121−2131.

(11) Xiao, Y. C.; Xie, J.; Yu, M.; Liu, M.; Ran, J.; Xi, Z.; Li, W.; Huang, J. *Chin. Chem. Lett.* **2011**, *22*, 1457−1460.

(12) Xiao, Y. C.; Lei, J.; Liu, M.; Yu, M.; Ran, J.; Xie, J.; Li, W.; Huang, J. *Helv. Chim. Acta* **2012**, *95*, 327−332.

(13) Li, W.; Wang, S. S.; Feng, J. T.; Xiao, Y. S.; Xue, X. Y.; Zhang, H.; Wang, Y. Q.; Liang, X. M. *Magn. Reson. Chem.* **2009**, *47*, 902−908.

(14) Sy, L. K.; Brown, G. D. *Magn. Reson. Chem.* **1997**, *35*, 424−425.

(15) Koo, H. J.; Gang, D. R. *PLoS One* **2012**, *7*, e51481.

(16) Tuvi-Arad, I.; Avnir, D. *Chem.—Eur. J.* **2012**, *18*, 10014−10020.

(17) Wang, J.; Chen, Z. Y.; Yan, B. C.; Ji, R. Y. *Chin. J. Med. Chem.* **1990**, *1*, 49−53.

(18) Mukherji, S. M.; Bhattacharyya, N. K. *J. Am. Chem. Soc.* **1953**, *75*, 4698−4700.

(19) Qin, N. Y.; Yang, F. Q.; Wang, Y. T.; Li, S. P. *J. Pharm. Biomed. Anal.* **2007**, *43*, 486−492.

(20) Kreiser, W.; Körner, F. *Helv. Chim. Acta* **1999**, *82*, 1610−1628.

(21) Golding, B. T.; Pombo-Villar, E. *J. Chem. Soc., Perkin Trans. 1* **1992**, 1519−1524.

(22) Debie, E.; De Gussem, E.; Dukor, R. K.; Herrebout, W.; Nafie, L. A.; Bultinck, P. *ChemPhysChem* **2011**, *12*, 1542−1549.

(23) Xie, J. X. In *The Application of Infrared Spectroscopy in Organic Chemistry and Medicinal Chemistry*; Science Press: Beijing, 1987; p 331.

(24) Qu, Y.; Xu, F. M.; Gao, H. Y.; Zhi, J. C. Y.; Wu, L. J. *J. Shenyang Pharm. Univ.* **2009**, *26*, 523−526.

(25) Carman, R. M.; Rayner, A. C. *Aust. J. Chem.* **1994**, *47*, 195−202.

(26) Liu, D. Z.; Wang, F.; Liao, T. G.; Tang, J. G.; Steglich, W.; Zhu, H. J.; Liu, J. K. *Org. Lett.* **2006**, *8*, 5749−5752.

(27) Bifulco, G.; Gomez-Paloma, L.; Riccio, R. *Tetrahedron Lett.* **2003**, *44*, 7137−7141.

(28) Chini, M. G.; Jones, C. R.; Zampella, A.; D'Auria, M. V.; Renga, B.; Fiorucci, S.; Butts, C. P.; Bifulco, G. *J. Org. Chem.* **2012**, *77*, 1489−1496.

(29) Rho, J. R.; Hwang, B. S.; Sim, C. J.; Joung, S.; Lee, H. Y.; Kim, H. J. *Org. Lett.* **2009**, *11*, 5590−5593.

(30) Forestieri, R.; Merchant, C. E.; de Voogd, N. J.; Matainaho, T.; Kieffer, T. J.; Andersen, R. J. *Org. Lett.* **2009**, *11*, 5166−5169.

(31) Huang, J. H.; Yang, J. R.; Zhang, J.; Yang, J. *J. Am. Chem. Soc.* **2012**, *134*, 8806−8809.

(32) Liu, L.; Bruhn, T.; Guo, L.; Götz, D. C.; Brun, R.; Stich, A.; Che, Y.; Bringmann, G. *Chem.—Eur. J.* **2011**, *17*, 2604−2613.

(33) Rocha, D. F. O.; Hamilton, K.; Gonçalves, C. C. S.; Machado, G.; Marsaioli, A. J. *J. Nat. Prod.* **2011**, *74*, 658−663.

(34) Kim, H. J.; Ruszczycky, M. W.; Choi, S. H.; Liu, Y. N.; Liu, H. W. *Nature* **2011**, *473*, 109−112.

(35) Zhao, C.; Yin, S. T.; Dong, Y. H.; Guo, X.; Fan, L. H.; Ye, M.; Hu, H. B. *Autophagy* **2013**, *9*, 196−207.

(36) Matthes, H. W. D.; Luu, B.; Ourisson, G. *Phytochemistry* **1980**, *19*, 2643−2650.

(37) *Sybyl Software*, version X 1.1; Tripos Associates Inc., St. Louis, MO, 2010.

(38) Bruhn, T.; Hemberger, Y.; Schaumlöffel, A.; Bringmann, G. *SpecDis*, version 1.51; University of Wuerzburg, Germany, 2011.

(39) Frisch, M. J.; Trucks, G. W.; Schlegel, H. B.; Scuseria, G. E.; Robb, M. A.; Cheeseman, J. R.; Scalmani, G.; Barone, V.; Mennucci, B.; Petersson, G. A.; Nakatsuji, H.; Caricato, M.; Li, X.; Hratchian, H. P.; Izmaylov, A. F.; Bloino, J.; Zheng, G.; Sonnenberg, J. L.; Hada, M.; Ehara, M.; Toyota, K.; Fukuda, R.; Hasegawa, J.; Ishida, M.; Nakajima, T.; Honda, Y.; Kitao, O.; Nakai, H.; Vreven, T.; Montgomery, J. A., Jr.; Peralta, J. E.; Ogliaro, F.; Bearpark, M.; Heyd, J. J.; Brothers, E.; Kudin, K. N.; Staroverov, V. N.; Kobayashi, R.; Normand, J.; Raghavachari, K.; Rendell, A.; Burant, J. C.; Iyengar, S. S.; Tomasi, J.; Cossi, M.; Rega, N.; Millam, N. J.; Klene, M.; Knox, J. E.; Cross, J. B.; Bakken, V.; Adamo, C.; Jaramillo, J.; Gomperts, R.; Stratmann, R. E.; Yazyev, O.; Austin, A. J.; Cammi, R.; Pomelli, C.; Ochterski, J. W.; Martin, R. L.; Morokuma, K.; Zakrzewski, V. G.; Voth, G. A.; Salvador, P.; Dannenberg, J. J.; Dapprich, S.; Daniels, A. D.; Farkas, O.; Foresman, J. B.; Ortiz, J. V.; Cioslowski, J.; Fox, D. J. *Gaussian 09*, revision B.01; Gaussian Inc.: Pittsburgh, PA, 2010.

(40) Debie, E.; Bultinck, P.; Nafie, L. A.; Dukor, R. K. *CompareVOA*; BioTools Inc.: Jupiter, FL, 2010.